NTNU

Norwegian University of
Science and Technology

Modeling and Control of Temperature in a Compartment Jet Fire

Hedda Moe Sandvik

Master of Science in Cybernetics and Robotics
Submission date: January 2017
Supervisor: Jan Tommy Gravdahl, ITK
Co-supervisor: Reidar Stølen, SP Fire Research
Christian Sesseng, SP Fire Research

Norwegian University of Science and Technology
Department of Engineering Cybernetics

Summary

Jet fires pose serious safety hazards in situations where pressurised gas tanks are stored close together. A jet fire originating from one tank will likely damage another and lead to additional fires and even explosions. To prevent this from happening, equipment has to built to be able to endure the high heat fluxes produced in jet fires. SP Fire Research has developed a test procedure where equipment can be tested for jet fires producing heat fluxes of 350 kW/m^2.

This thesis has worked towards implementing automatic control of the temperature in the oven of this test set up. The temperature inside the oven is regulated by fans supplying the oven with additional air, a change in fan frequency leads to a change in temperature. The oven has prior to this thesis been built in two different ways, resulting in two systems with different dynamics, one over ventilated and one under ventilated.

Mathematical models were created to decide the relationship between fan inputs and the oven temperature in both systems. This was done by modifying an existing compartment fire temperature model to accommodate the effects the jet fire has on the system, as well as the bigger openings in the compartment (oven). The resulting models were then verified by comparing simulations to data from previous tests. With satisfying comparison results, the models were used to test different control schemes through simulation. These simulations suggested that PI control should work in both systems. Consequently, PI control was tested in the over ventilated system. The results were conclusive with simulations, and the PI control was verified as a suitable control scheme for the over ventilated system. It is expected to work just as well in the under ventilated system, though it has not yet been tested.

In addition to the main objective of temperature control, some additional functionalities have been assessed. Reference control schemes are suggested, and a way to automatically detect and terminate faulty thermocouples. The advantages and disadvantages of the two systems were reviewed. The over ventilated system was suggested as the favorable choice, but should be continuously reviewed through changing weather conditions as it is more affected by weather than the under ventilated system, as the test rig is situated outside.

Sammendrag

Jetbrann utgjør en alvorlig sikkerhetsrisiko i situasjoner der gasstanker under høyt trykk er lagret tett sammen. Om en jetbrann oppstår fra en tank, vil denne brannen mulig skade andre tanker og føre til flere branner eller til og med eksplosjoner. For å hindre at dette skal skje må utstyr som tåler de høye varmefluksene som jetbranner produserer bli installert. SP Fire Research har utviklet en testprosedyre som kan teste utstyrs motstandsdyktighet til jetbrann som produserer varmeflukser av 350 kW/m^2.

Denne avhandlingen har jobbet mot å implementere automatisk styring av temperatur i ovnen i dette testoppsettet. Temperaturen inne i ovnen reguleres ved hjelp av vifter som forsyner jetbrannflammen med ytterligere luft, en endring av viftefrekvens fører derfor til en endring av temperatur. Ovnen har blitt bygget på to forskjellige måter i forkant av denne avhandlingen, noe som resulterer i to systemer med forskjellig dynamikk, en overventilert og en underventilert.

Matematiske modeller har blitt utviklet for å bestemme forholdet mellom vitfepådrag og ovnstemperat i begge systemene. Dette ble gjort ved å tilpasse en eksisterende rombrannmodell så den passer tilstandene i en jetbrann. De resulterende modellene ble så verifisert ved å sammenligne simuleringer med data fra tidligere tester. Med tilfredstillende simuleringsresultater kunne modellene brukes til å teste ulike regulatorer gjennom videre simulering. Disse simuleringene tydet på at PI-regulering burde fungere fint i begge systemene. Følgelig ble PI-regulering testet i det overventilerte systemet, med resultater som overensstemte med simuleringene. PI-regulering ble dermed bekreftet som en egnet regulator for det overventilerte systemet. Det forventes å fungere like godt i det underventilerte systemet, men dette har ikke enda blitt testet.

I tillegg til hovedmålet om temperaturkontroll har noen ekstra funksjonaliteter blitt vurdert. Reguleringsalgoritmer for referansekontroll er foreslått, og en måte å automatisk oppdage og terminere defekte termoelementer. Fordeler og ulemper med de to forskjellige systemene er veid opp mot hverandre, hvor det overventilerte systemet seiret som det beste valget. Dette burde derimot vurderes løpende siden testriggen befinner seg utendørs og det overventilerte systemet er mer påvirket av vær enn det underventilerte.

Preface

The following study was done in most part during the fall of 2016 as the last step towards a masters degree in Engineering Cybernetics at the Norwegian University of Science and Technology (NTNU). It was performed in collaboration with SP Fire Research, a company researching, you guessed it, fires. The project was formed by the company's aspiration for automatic temperature control in one of their research test rigs. To this date said test rig is controlled manually as the test is conducted.

My history with SP Fire Research started in early 2016, when I joined the project. In the spring of 2016 I worked on a project thesis[35] that taught me a lot about the science behind fires, and created the basis to this master thesis. Some of the work from the project thesis is therefore included in this master thesis.

My supervisors throughout the year has been Professor Jan Tommy Gravdahl from the Department of Engineering Cybernetics at NTNU, and Christian Sesseng and Reidar Stølen from SP Fire Research. They have helped me throughout the process through both regular and irregular meetings, where we have discussed the project and together continuously determined the next step in the process towards automatic temperature control. I would like to thank all three of them for their guidance and collaboration.

Trondheim, January 2017

Hedda Moe Sandvik

Table of Contents

List of Tables

List of Figures

Nomenclature

α_W	Convective heat transfer coefficient [kW/m^{2}K]
ΔH_a	Heat of combustion per unit mass of air [kW/m^{2}K]
ΔH_p	Heat of combustion of propane [kW/m^{2}K]
ϕ	Heat flux [kW/m^2]
ϕ_{avg}	Heat flux running average [kW/m^2]
ϕ_{ref}	Heat flux reference value [kW/m^2]
ρ_∞	Density of ambient air [kg/m^3]
σ	Stefan-Boltzmann constant [kW/m^{2}K^4]
ε_W	Compartment boundary emissivity
A_f	Cross sectional area of fan shafts [m^2]
A_W	Area of compartment boundaries [m^2]
A_{op_h}	Area of horizontal ventilation opening [m^2]
A_{op_v}	Area of vertical ventilation opening [m^2]
A_{op}	Area of ventilation opening [m^2]
c_p	Specific heat of air [kj/kgK]
dz_{lim}	Dead zone limit [%]
e	Temperature error [C]
e_ϕ	Heat flux error [kW/m^2]
H_{op_v}	Height of vertical opening [m^3]

k_a	Scaling coefficient Q_C
k_a	Under ventilated combustion scaling coefficient
K_b	Back-calculation coefficient
K_c	Proportional gain
k_p	Over ventilated combustion scaling coefficient
$k_r p$	Reference control proportional gain
k_W	Scaling coefficient $\dot{T}_W$
k_W	Wall temperature approximation constant
m_a	Mass flow rate of air entering the compartment [kg/s]
m_f	Air mass flow rate contributed by fans [kg/s]
m_g	Mass flow rate of gas out of compartment [kg/s]
m_p	Mass flow rate of propane entering the compartment [kg/s]
m_{fv}	Forced ventilation air mass flow rate [kg/s]
m_{nv}	Natural ventilation air mass flow rate [kg/s]
PB	Proportional band
Q_C	Heat energy released in combustion [kW]
Q_R	Radiative heat loss through ventilation opening [kW]
Q_V	Heat loss due to ventilation [kW]
Q_W	Heat loss to compartment boundaries [kW]
T	Flame temperature [K]
T_α	Average temperature of T and T_W [K]
T_α	Convective heat transfer coefficient
T_∞	Ambient temperature [K]
T_d	Derivative action time
T_i	Integral action time
T_W	Oven wall temperature [K]
T_{ref}	Reference temperature [C]
u	Fan input [%]
u_r	Temperature reference control input [K]
V	Inner oven volume [m^3]

Chapter 1

Introduction

Highly flammable hydrocarbon gases are commonly stored in pressurised tanks and transported through pipes under high pressure. In the event of leakage, the pressure in the container will cause gas to be discharged at high velocities. If this high velocity gas is ignited, a turbulent diffusion flame develops, creating a vicious fire plume. Thus, a jet fire is born.

Although jet fires are generally smaller than other types of fires, they can be locally very intense. The center of the fire plume is very concentrated and produces higher heat fluxes than experienced in most other fires. If this plume impinges on other equipment (e.g. tanks or pipes), it may cause damage that can lead to additional, more substantial safety hazards. The chance that additional fires or even explosions occur are regrettably high. The risk of this ”domino effect” [23] is particularly relevant to all industries where gas pipes and containers are positioned close together, such as on oil rigs and tankers. Jet fires have previously lead to oil rig disasters such as the Piper Alpha incident[18].

In the interest of reducing the potential hazards caused by jet fires, proper equipment has to be installed. To ensure that said equipment can tolerate the severe heat fluxes produced in a jet fire, it has to be tested under the right conditions. The jet fire test standard ISO 22899-1 [5] has therefore been developed to test equipments resistance to heat fluxes of 250 kW/m^2. SP Fire Research is however even more ambitious, as they offer a test producing a jet fire with heat fluxes of 350 kW/m^2.

1.1 Background

The test standard ISO 22899-1 features a jet fire created from a fuel ejected with mass flow rate of 0.3 kg/s impinging on the test piece and a surface behind it. This set up typically reaches temperatures up to 1200° degrees and heat fluxes of 250 kW/m^2. On a quest to offer even more extensive testing, SP Fire Research set a goal of reaching temperatures of 1300°C and heat fluxes of 350 kW/m^2. The first step towards achieving this was building

walls and a roof around the jet fire to shield the flame from the environments, as the test rig is situated outside. It was discovered that with too much isolation, the flame did not have access to enough oxygen to combust properly and produce the desired temperatures. Instead of trying to build the perfect oven for each test according to the current weather conditions, fans were added so they were able to regulate the temperature inside the oven during the test. The resulting configuration is referred to as the under ventilated system. Up to now, the temperature has been controlled manually by changing the frequency of the fans. The next step goal in the development of this test rig is thus implementing a controller that automatically regulates the oven temperature to the desired value.

The objective of this test is to expose the test piece to heat fluxes of 350 kW/m^2, corresponding to a temperature of 1300°C, from five minutes into the test. If the oven should hold a temperature under 1300°C for some time, the reference temperature is set a bit higher so that the average heat flux by the end of the test reaches 350 kW/m^2. Temperatures above 1350°C are very undesirable, so this is the highest reference temperature used and an important constraint.

1.2 Previous work

Prior to this master thesis, I finished a project thesis on the same project. In this thesis, a mathematical model for the under ventilated system described above was created and tested through simulations. As the project thesis is not publicly published, the most essential results from the project thesis is also included in this master thesis.

1.3 Thesis objective

The motivation behind this thesis is to implement automatic temperature control in the test rig developed by SP Fire Research. When work on this thesis started, a new oven configuration with bigger ventilation openings had just been tested with positive results. This configuration is referred to as the over ventilated system. As the dynamics of this oven differs substantially from the under ventilated system, the first objective of this thesis became to alter the under ventilated model created in the project thesis to an over ventilated model. The next objective was then to study both models response to different control schemes through simulations, and reviewing which system was favorable of the two. After finding a satisfactory control scheme through simulations, experiments with the selected controller in the actual test rig must be done to verify the simulation results. If the controller works well in these tests, it can be implemented into the system and thus the goal of this project is reached.

These were the objectives set at the beginning of the study. During the study some experiences with the system motivated two new objectives. The over ventilated system typically uses a long time to reach 1300°C. To compensate for this, the temperature has been controlled to a higher value. Thus the heat flux imposed on the test piece averages to 350 kW/m^2 over the duration of the test. For this to happen automatically, a temperature ref-

erence controller has to be implemented. Thus the objective of researching temperature reference control was set.

In many of the tests it has been experienced that thermocouples fail. When they do, they produce faulty data. This faulty data could possibly disturb the controller and result in inaccurate control. This motivated the objective of finding a way to automatically detect and terminate faulty thermocouples.

1.4 Structure of the report

The rest of the report is structured as follows: Chapter 2 gives an introduction to the physics related to fires. Chapter 3 gives a description of the properties and dimensions of the system. The various mathematical models developed during this project is presented in chapter 4, and their response to different temperature control schemes in chapter 5. PI control was then tested, and the results are shown in chapter 6. In chapter 7 some suggestions to reference control schemes are presented, and chapter 8 gives a brief analysis of thermocouple failure. Last but not least, discussion on various topics are found in chapter 9 and the conclusion is given in chapter 10.

Chapter 2

Introduction to Fire Dynamics

In this chapter the basic physics of fires is presented. This includes the theory of combustion as well as modes of heat transfer. Other dynamics that effect fires have been omitted as it is not vital to understand the final mathematical model. This chapter is in its whole copied from the corresponding project thesis[35] written prior to this master thesis.

2.1 Combustion

A fire develops as a result of uncontrolled combustion. Combustion is a reaction between fuel and oxygen which produces energy in form of heat and products of various kinds. In most cases this reaction results in a visible flame depending on the fuel and the amount of oxygen available. For combustion to occur, a certain amount of energy has to be available to trigger the reaction. This energy is dependant on the reactants and is used to break the molecules bonds so that new compounds can be formed. The chemical reaction of combustion can be expressed by the general chemical equation 2.1.

$$fuel + oxygen \xrightarrow{energy} products \tag{2.1}$$

These three components needed for combustion to occur are often termed the fire triangle[29] illustrated in Figure 2.1 (a). Further research has however proved that these three components are not sufficient in sustaining a fire. To keep the chain reaction going, free radicals have to be present in the combustion zone[15]. The fire triangle can therefore been expanded to a fire tetrahedon, as seen in Figure 2.1 (b).

2.1.1 Combustion of propane

Propane is a hydrocarbon consisting of three carbon and eight hydrogen atoms, forming C_3H_8. This gas is highly flammable and burns freely in air at concentrations between 2.1

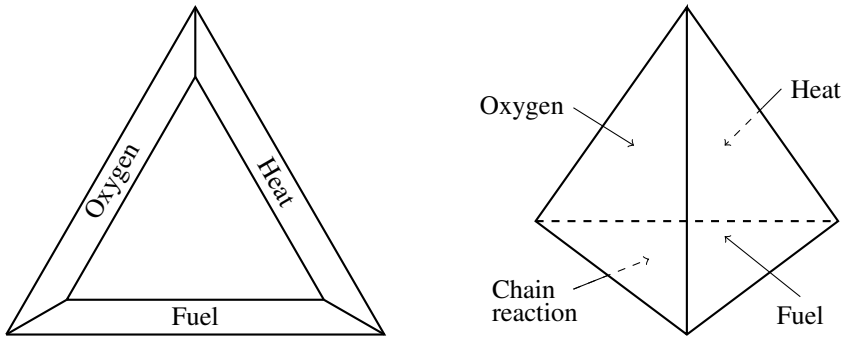

Figure 2.1: (a) Fire triangle and (b) tetrahedron.

and 9.5 Vol %[20].

When an abundance of oxygen is available, complete combustion occurs. In this reaction the only products are water and carbon dioxide, as seen in equation 2.2. This reaction releases the maximum amount of energy.

$$C_3H_8 + 5 \cdot O_2 \rightarrow 3 \cdot CO_2 + 4 \cdot H_2O \tag{2.2}$$

When the combustion is limited by oxygen, propane burns incompletely to also form carbon monoxide and/or soot by the following chemical equations

$$2 \cdot C_3H_8 + 9 \cdot O_2 \rightarrow 4 \cdot CO_2 + 2 \cdot CO + 8 \cdot H_2O \tag{2.3}$$

$$C_3H_8 + 2 \cdot O_2 \rightarrow 3 \cdot C + 4 \cdot H_2O \tag{2.4}$$

Incomplete combustion releases less energy and the biproducts can affect the fire negatively. It is therefore undesirable, yet practically impossible to avoid in diffusion[1] flames.

2.2 Modes of heat transfer

Once heat energy has been released by the combustion process, this energy will spread and be transferred to its surroundings. There are three ways this energy can be transferred[22], through solid objects by conduction, through fluids to a solid surface by conduction, or though space by radiation. Heat transfer is measured in heat flux, denoted by q'' (W/m^2). Heat rate, Q (W), can be found by multiplying flux with the total area A affected.

$$Q = q'' \cdot A \tag{2.5}$$

[1] A diffusion flame refers to a flame where fuel and oxygen is mixed (by diffusion) in the combustion zone. In the contrasting premixed flame, fuel and oxygen is mixed before reaching the combustion zone.

2.2.1 Conduction

Conduction is a mode of heat transfer through solid objects. Fouriers law[22] expresses conduction as

$$\boldsymbol{q}'' = -k\Delta T = -k(\boldsymbol{i}\frac{\partial T}{\partial x} + \boldsymbol{j}\frac{\partial T}{\partial y} + \boldsymbol{k}\frac{\partial T}{\partial z}) \tag{2.6}$$

Limiting this vectors to the x component and assuming a linear temperature distribution throughout the object, this expression reduces to

$$q''_x = -k\frac{T_1 - T_2}{L} \tag{2.7}$$

The parameter k is known as the thermal conductivity (W/m·K) and is a transport property of the material heat passes through. Figure 2.2 illustrates conduction in one dimension.

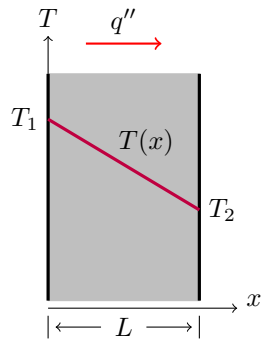

Figure 2.2: One-dimensional heat transfer by conduction

2.2.2 Convection

Convection describes the heat transfer between a moving fluid and a solid surface at two different temperatures. Because of the velocity gradient near the surface there will be a corresponding temperature gradient varying from T_s, the temperature of the solid surface, to T_∞, the temperature of the fluid. This region is called the thermal boundary layer and is illustrated in Figure 2.3.

The convective heat transfer process can take effect in many different ways, but regardless of this the rate equation is always expressed by Newtons law of cooling[22] as

$$q'' = h(T_s - T_\infty) \tag{2.8}$$

where h (W/m^2·K), the convection heat transfer coefficient determines the proportionality between convective heat flux (W/m^2) and the difference between T_s and T_∞. The convection heat transfer coefficient is determined by conditions in the boundary layer.

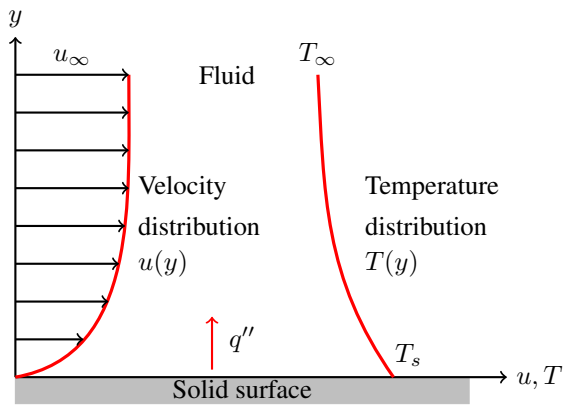

Figure 2.3: Boundary layer development in convective heat transfer.

2.2.3 Radiation

Radiation is heat energy emitted by matter at a nonzero temperature. In contrast to conduction and convection which requires material medium to transfer heat, radiation is heat transferred by electromagnetic waves and therefore do not. A simplified expression of radiative heat transfer between two energy sources, e.g. two surfaces as illustrated in Figure 2.4, is given by equation 2.9.

$$q'' = \varepsilon\sigma(T_1^4 - T_2^4) \tag{2.9}$$

where σ is the Stefan Boltzmann constant (σ = $5.67 \cdot 10^{-8}$W/m·K^4) and ε is a radiative property called emissivity with a value ranging from 0 to 1, 1 corresponding to ideal blackbody radiation[22].

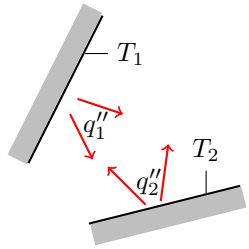

Figure 2.4: Radiation between two surfaces at temperatures T_1 and T_2

Chapter 3

System overview

This chapter gives a description of the system, specifically the structure of the oven, the controllable system inputs, and the configuration of measuring devices collecting data. The different system configurations, meaning the size and situation of the ventilation openings in the different systems are also presented.

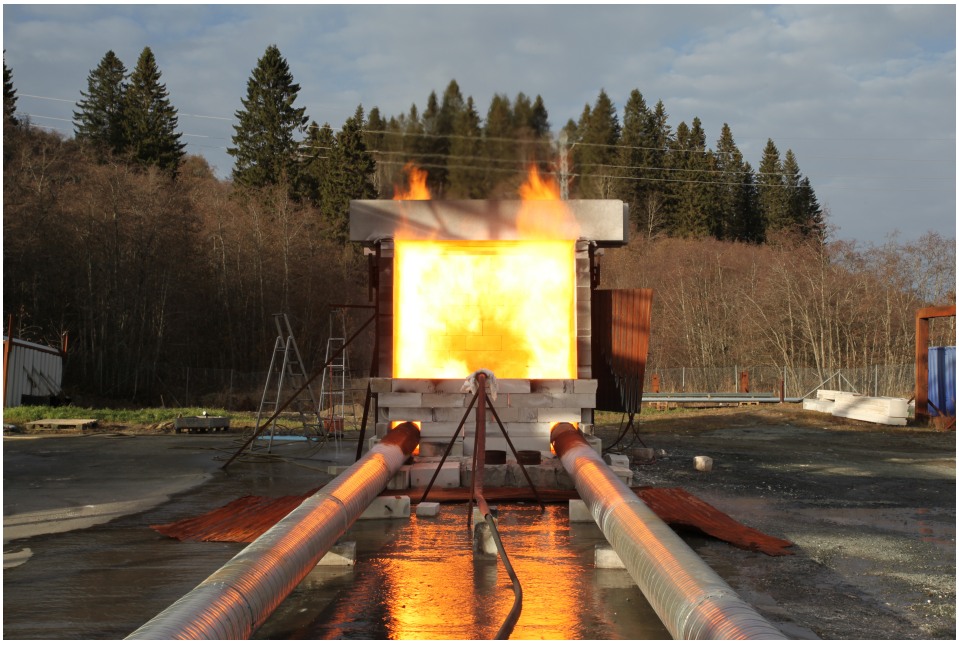

Figure 3.1: The test rig in action.

3.1 Oven structure

The oven the tests are conducted in is built in a cubic fashion. Its inner volume measures 2.6 meters wide, 3 meters tall and 2.8 meters deep, see the illustration in figure 3.2. The ventilation openings are in the front wall and/or ceiling and are of varying size. It is built mainly out of a material called autoclaved aerated concrete, also known as ”Siporex”. This material is concrete produced such that small air bubbles are formed on the inside of the material[9]. The presence of air bubbles makes it a great thermal insulator[8], and the porous structure provides exceptional fire resistance. It is also fairly lightweight and easy to cut, making it easy to work with. It is consequently the perfect material for the job. It is however not invincible, so the Siporex blocks have to be replaced after long exposure to high temperatures. The blocks normally last for several tests, making the properties of the oven walls a bit different from test to test.

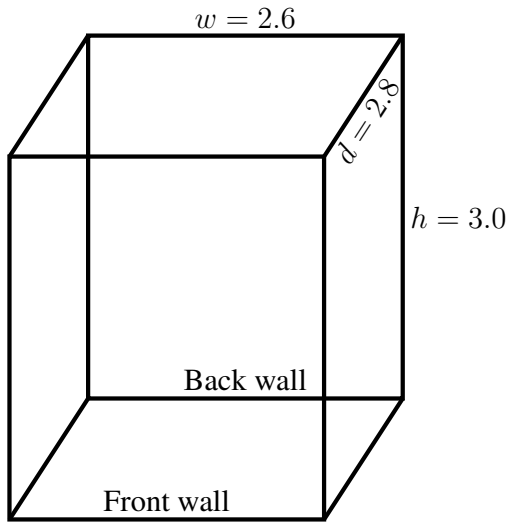

Figure 3.2: The ovens inner dimensions.

3.2 The test piece

The piece of equipment being tested is situated against the back wall of the oven. It is placed in the area where the jet fire impinges on the back wall. In some cases, the piece of equipment being tested is a door or a wall of some kind. In these tests the back wall of siporex is simply replaced by the test piece.

3.3 Controllable inputs

To recreate a jet fire, a fuel in gas form has to be released through a small opening at a high velocity. The fuel used in this experimental setup is propane, and it is supplied to the

oven through a nozzle situated in the middle of the oven, the pipe connected to the nozzle protruding from the front wall. The resulting flame then impinges on the test piece and the back wall. The velocity of the propane supplied is PID controlled with a reference value of 0.3 kg/s, and this constitutes one of the systems two controllable inputs.

The other controllable input, and the one actively used to control the temperature inside the oven, is the air supplied through fans. There are two separate fans supplying air to the oven through corresponding fan shafts with a radius of 20 cm. The fan shafts discharge air through the bottom corners of the front wall, see figure 3.3. The fans operate in a frequency range of 0-50 Hz, and are controlled by Altivar 61 frequency inverters[6]. The input signal is recorded in the data logging system as a percentage of full efficiency (50 Hz).

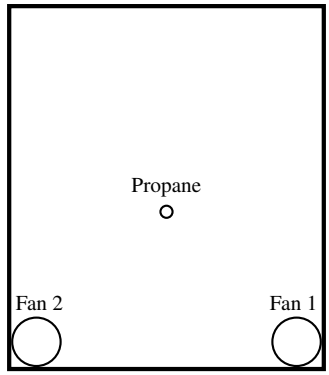

Figure 3.3: Location of the fan and propane inputs on the front wall.

3.4 Temperature measurements

Temperature measurements inside the oven are for the most part measured with type K thermocouples. These thermocouples are able to measure temperatures up to 1370°C[4], making them perfectly suitable in most cases. In some cases platinum thermocouples have been used, these are able to record even higher temperatures.

The thermocouples are placed in the area where the highest temperatures are expected. There are normally six thermocouples in a configuration with three thermocouples at different heights at each side, as seen in figure 3.4. The vertical distance between the thermocouples may vary from test to test.

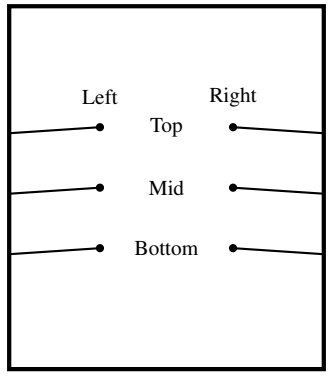

Figure 3.4: Thermocouple configuration inside the oven. The black dots denote the measurement points.

3.5 Ventilation openings

The response of the system depends largely on how the oven is built. The size of the ventilation openings determines if the system is over or under ventilated. This difference has vast consequences on how the system is controlled, and each configuration comes with advantages and disadvantages. This thesis covers tests with three different oven builds featuring three different configurations of ventilation openings and sizes. Two of these are over ventilated systems and are fairly similar, the last is the under ventilated system.

3.5.1 Under ventilated system

Until the summer of 2016, the oven was built for under ventilated control. This build features a ventilation opening in the front wall, see figure 3.5. This system by itself struggles to provide the flame inside the oven with sufficient oxygen. The flame consist of a higher fraction of incomplete combustion, making its temperature lower than if the flame was properly ventilated (complete combustion). Actuating the fans delivers more air to the system, and consequently more oxygen to aid in combustion. This added oxygen increases the rate of complete combustion and more energy is released to the system. Thus increasing the fan input will also increase the temperature inside the oven.

Measurement data from under ventilated tests can be found in Appendix B.

3.5.2 Over ventilated system

In the early parts of the summer 2016, the possibility of building the oven with bigger ventilation openings was explored. The idea was to allow the flame enough air to completely combust, and then use the fans to increase the mass flow through the system. Higher fan inputs therefore means higher rates of heat loss from the system, leading to lower temperatures. Two different over ventilated systems have been explored with different opening sizes. Both feature a bigger front opening than the under ventilated system, and

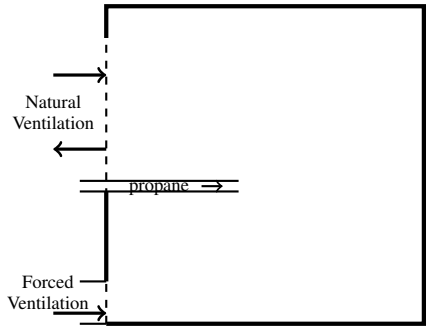

Figure 3.5: Side view of the under ventilated oven build.

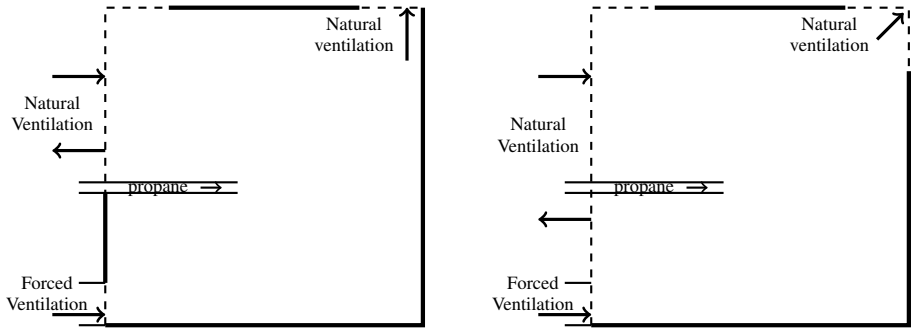

(a) Build with smaller openings.

(b) Build with larger openings.

Figure 3.6: Sideview of the two over ventilated oven builds used in previous tests.

an additional opening in the corner between the roof and the back wall. The two builds differ slightly in the size of these openings, see figure 3.6. The build in 3.6a was used on 13.05.2016 and 01.07.2016, and the build in 3.6b on 28-30.06.2016.

Measurement data from over ventilated tests can be found in Appendix C.

3.6 Effects of weather

The entirety of the test rig is situated outside, as seen in figure 3.1. The effects of weather therefore has to be factored in to evaluate the response of the system. Wind might affect the ventilation rates of the system, and the walls of the oven will store water when it rains. During winter, the oven will likely be covered with snow, possibly affecting the systems response. However, none of the provided measurement data is from tests conducted in the winter. The data from under ventilated tests feature little to no wind. This means the systems response depending on weather conditions cannot be properly assessed.

Chapter 4

Mathematical modelling

In this chapter, all the mathematical models created in the process of writing this master thesis and the proceeding project thesis[35] are presented. The new models are based on the under ventilated model was created in the project thesis. Simulations of the models are compared to measurement data. Simulations are done using MATLABs Simulink program.

4.1 Merging jet and compartment fires

In the field of jet fire modeling, a vast amount of modeling and temperature estimation has been done in the spacial plane. In fact, the British Health & Safety Executive has published a CFD model describing the exact jet fire used in the experiment in detail[11]. While this provides an insight into the physical characteristics and properties of jet fires, these kind of models are not applicable to solve the problem at hand. To control a process, it has to be analyzed in the time domain, and little to no jet fire modeling has been done with respect to time.

The solution to this problem was found by looking at it from a completely different perspective. The control input to the system is essentially ventilation rates into a compartment fire, namely the jet fire inside the oven. When it comes to compartment fires (also called room or enclosure fire), a great deal of modeling has been done to estimate the potential temperatures that can occur in a compartment fire[37][39][32]. These temperature estimates are based on concepts such as mass and energy balance, which are also applicable to process modeling to test the systems response to control. While none of the articles specifies jet fire as the source of combustion, the same principles are applicable. This is how the basis for the temperature model was found. The models are largely based on the article *A Simple Predictive Method for Room Fire Behaviour* by Matsuyama et.al.[24].

There are some notable differences between the jet fire inside the oven and a typical compartment fire. The first is the size of the ventilation openings. In a typical compartment

fire model, the ventilation openings are quite small compared to the compartment itself, typically mimicking a door or a window. In the jet fire oven the ventilation opening covers a much bigger portion of the compartment. Naturally, this affects the temperatures that accumulated inside the compartment.

The other notable difference is that typical compartment fires base the calculation of the ventilation rates on the concept of a two-layered model. This assumes that the upper part of the compartment is covered in a hot layer of gas produced by the fire, and the lower part consist of more or less fresh air. The ventilation rates in and out of an opening is then computed based on the thickness of the hot upper layer. In the jet fire oven this two-layered model is not applicable. This is likely an effect of the characteristics of a jet fire. The jet fire flame creates turbulence that leads to better mixing of air and fuel throughout the oven. The high velocity of the propane input and the larger ventilation openings also lead to a faster mass flow rate throughout the system, which prevents a hot gas upper layer to form. It is therefore not at all rare to observe higher temperatures at the bottom of the rig than at the top. The point where the highest temperature is measured seems arbitrary in most tests.

The type of ventilation in the jet fire oven is also quite unique; it is a combination of both natural and forced (or mechanical) ventilation. The ventilation applied in the previously cited articles is natural ventilation through windows or doorways. Models based on forced ventilation were also found[17], but none merging the two ventilation types. However, the effects of different kinds of ventilation on compartment fires have been heavily researched[13][14] [26][30]. These studies provide an insight into the ventilation types, but is more or less rendered obsolete by the dynamics in the jet fire oven differing from a typical compartment fire.

4.2 Under ventilated model

The under ventilated temperature model was created in the project thesis written previously to this master thesis. This section is therefore largely copied from the project thesis[35].

This under ventilated model completely neglects the effects of natural ventilation, and assumes all the oxygen supplied to the system via forced ventilation instantaneously aids in combustion.

4.2.1 The temperature state equation, $\dot{T}$

To form a temperature state equation for the system, the concepts of energy and mass conservation are used, as well as the state equation $\rho T = \rho_\infty T_\infty$.

$$\begin{aligned}\frac{d}{dt}(c_p\rho(T-T_\infty)V) &= Q_C - Q_W - Q_R - Q_V \\ &= Q_C - Q_W - Q_R - c_p m_g(T-T_\infty) \qquad (4.1)\end{aligned}$$

$$\frac{d}{dt}(\rho V) = m_a + m_p - m_g \qquad (4.2)$$

The energy conservation equation in the test rig is given by equation 4.1. Q_C corresponds to the energy released during combustion, Q_W the heat loss to the walls, Q_R is heat loss due to radiation through the opening, and Q_V is the heat loss due to ventilation.

In the mass conservation equation 4.2, the volume V and density ρ inside the oven is assumed constant, so that $m_g = m_a + m_p$.

An expression for the temperature dynamics can be found by combining these three equations. The resulting temperature state equation is given by equation 4.3.

$$\dot{T} = \frac{T}{c_p \rho_\infty T_\infty V}(Q_C - Q_W - Q_R) - \frac{T}{\rho_\infty T_\infty V}(m_a + m_p)(T - T_\infty) \tag{4.3}$$

4.2.2 Air mass flow rate through forced ventilation, m_a

Given the assumption that the air consumed in the combustion process is exclusively delivered by forced ventilation, the air mass flow rate into the system m_a is a function of the fan input u. To find this relationship, an experiment was conducted on April 13th 2016. The differential pressure was measured with a bi-directional probe situated in the left fan shaft (fan 1) 1.5 meters from the opening into the test rig. The bi-directional probe is a robust and versatile measuring device, as it is insensitive the angle of the approaching flow (0-50 degrees)[12][28]. It measures stagnation pressure in the chamber upstream of the flow, and the downstream pressure in the back chamber, see Figure 4.1a.

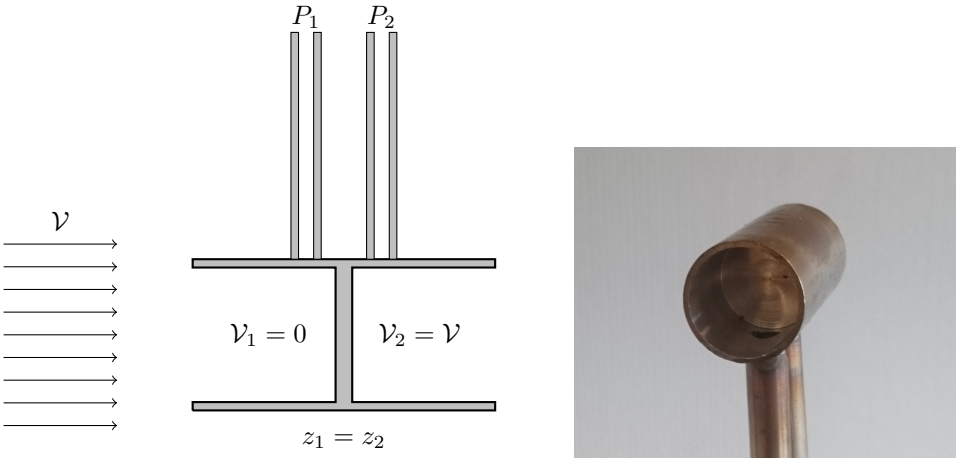

(a) Illustration of the probes characteristics.

(b) The probe

Figure 4.1: Bi-directional pressure probe

By modifying Bernoulli's equation 4.4[16] this information can be used to derive an expression for the velocity through the pipe, eq. 4.5, and thus the flow rate, eq. 4.6.

$$\frac{P_1}{\rho g} + \frac{\mathcal{V}_1^2}{2g} + z_1 = \frac{P_2}{\rho g} + \frac{\mathcal{V}_2^2}{2g} + z_2 \tag{4.4}$$

$$\mathcal{V} = \sqrt{\frac{2\Delta P}{\rho}}, \quad \Delta P = P_1 - P_2 \tag{4.5}$$

$$m_f = \rho \mathcal{V} A_f = A_f \sqrt{2\rho \Delta P} \tag{4.6}$$

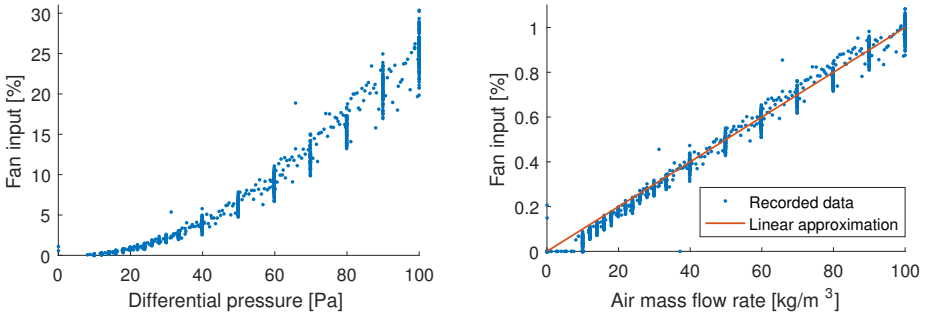

(a) Differential pressure recorded by the probe at different fan inputs.

(b) Mass flow rates at different fan inputs and a linear approximation (red).

Figure 4.2: Results of testing the fans.

The results of the experiment are shown in Figure 4.2. The mass flow rates at different fan inputs were calculated from the differential pressure recorded by the probe. As seen in figure 4.2b, a linear approximation $m_f = 0.01u$ expresses the relationship between fans and air mass flow rate adequately. Since there are two fans, the expression used in the model is

$$m_a = m_f = 0.02u \tag{4.7}$$

4.2.3 Heat energy released through combustion, Q_C

Regardless of the fuel consumed in combustion, the heat generated can be related to the mass of air consumed by a constant ΔH_a of about 3000 kJ/kg [25]. Under the assumption that all of the air supplied through the fans instantly reacts with propane, the expression for the heat energy released through combustion is given by equation 4.8.

$$Q_C = m_a \Delta H_a \tag{4.8}$$

Despite this being based on well defined theory and experimental data, when it was implemented the model simulation did not reach the desired temperatures. To correct this, a

scaling coefficient k_a was added to equation 4.8. It was tuned to $k_a = 1.5$ by comparing simulation and measurement data.

$$Q_C = k_a m_a \Delta H_a \tag{4.9}$$

4.2.4 Heat loss, Q_W and Q_R

The heat energy released by the combustion process suffers losses to its surroundings, namely the test rig consisting of walls, the test piece and the ventilation opening. The temperature at the wall surface is estimated by a first order approximation given in equation 4.10, and corresponds to the heat lost through the walls due to conduction.

$$\dot{T}_W = k_W(T - T_W) \tag{4.10}$$

The convective and radiative heat losses to the walls are expressed by equation 4.11, where A_W is the total area of the oven walls.

$$Q_W = \varepsilon_W \sigma A_W (T^4 - T_W^4) + \alpha_W A_W (T - T_W) \tag{4.11}$$

The convective heat transfer coefficient α_W is determined by [38] as equation 4.12.

$$\alpha_W = \begin{cases} 5 \cdot 10^{-3} & (T_\alpha \leq 300K) \\ (0.02T_\alpha - 1) \cdot 10^{-3} & (300K < T_\alpha < 800K)\ , \\ 15 \cdot 10^{-3} & (800K \leq T_\alpha) \end{cases} \quad T_\alpha = (T + T_W)/2 \tag{4.12}$$

The radiative heat loss through the ventilation opening is given by the following equation

$$Q_R = \sigma A_{op}(T^4 - T_W^4) \tag{4.13}$$

4.2.5 Complete model

Combining all of these equations results in the following complete model:

$$\dot{T} = \frac{T}{c_p \rho_\infty T_\infty V}(Q_C - Q_W - Q_R) - \frac{T}{\rho_\infty T_\infty V}(m_a + m_p)(T - T_\infty) \tag{4.14}$$

$$\dot{T}_W = k_W(T - T_W) \tag{4.15}$$

$$Q_C = k_a m_a \Delta H_a \tag{4.16}$$

$$Q_W = \varepsilon_W \sigma A_W (T^4 - T_W^4) + \alpha_W A_W (T - T_W) \tag{4.17}$$

$$Q_R = \sigma A_{op}(T^4 - T_W^4) \tag{4.18}$$

$$m_a = m_f = 0.02u \tag{4.19}$$

4.2.6 Model verification

The over ventilated model was verified by comparing its response to measurement data from the tests conducted from October 2015. The constants k_w and k_a were tuned to 0.07 and 0.3, respectively, in all simulations but the comparison to 22.10.15. In this simulation

the values $k_w = 0.3$ and $k_a = 1.4$ were used. The results of simulation is shown in figures 4.3 to 4.6 Note that the temperature axes are scaled from 1000°C as the initial transient is not an important part of the model verification, the interest lies in the operating area of about 1300°C.

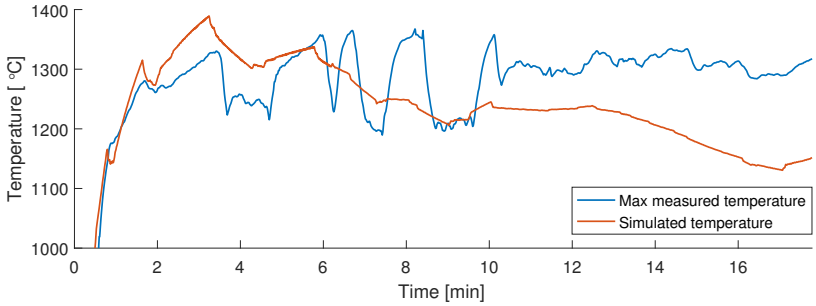

Figure 4.3: Measured max temperature and simulated temperature from 13.10.15.

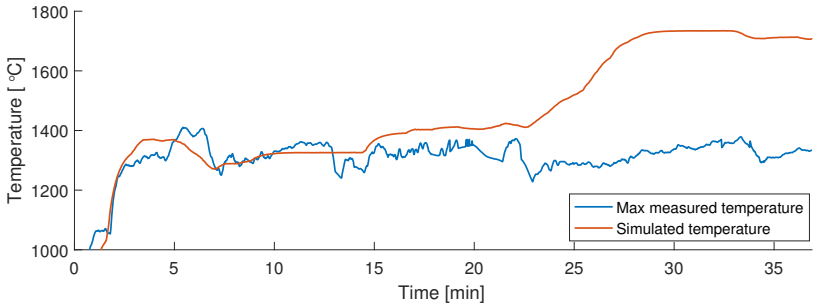

Figure 4.4: Measured max temperature and simulated temperature from 22.10.15.

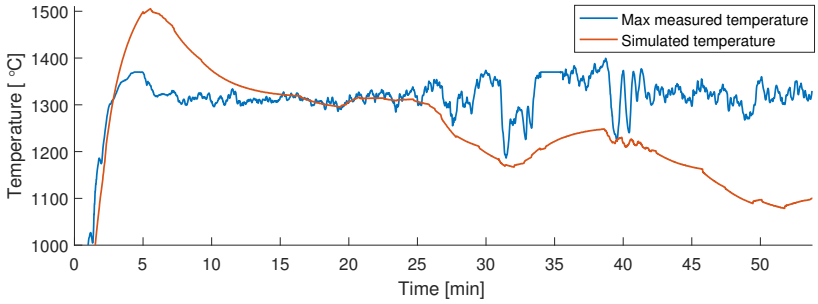

Figure 4.5: Measured max temperature and simulated temperature from 28.10.15.

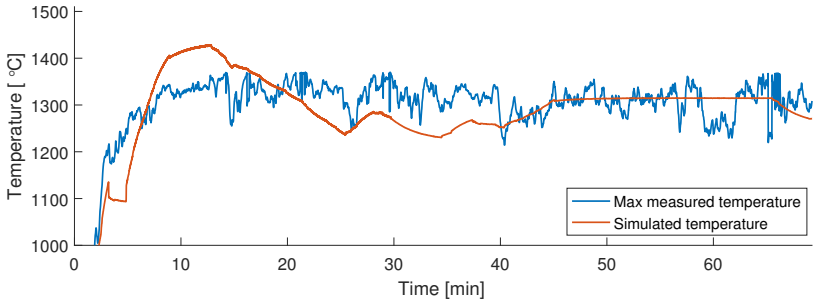

Figure 4.6: Measured max temperature and simulated temperature from 30.10.15.

4.3 Over ventilated model

The over ventilated rig configuration responds to fan input in a largely different manner than the under ventilated mathematical model predicts. Therefore, a new mathematical model had to be created to simulate the over ventilated system. The model presented in this section is based on the assumption that the system in itself is properly ventilated. Actuating the fans will then lead to an increased mass flow rate throughout the system, and hence decrease the temperature of the system.

4.3.1 Area of ventilation opening

The over ventilated system features two ventilation opening, both part vertical and horizontal. The horizontal and vertical parts of the openings have different characteristics. The total area of the opening, A_{op}, has therefore been split into two parameters, A_{op_v} and A_{op_h} corresponding to the vertical and horizontal parts, respectively. The total area of ventilation openings, A_{op}, is thus expressed as

$$A_{op} = A_{op_v} + A_{op_h} \tag{4.20}$$

4.3.2 Air mass flow rates

The under ventilated model in section 4.2 completely neglects the effects of natural ventilation. To include the over ventilated state into the model, natural ventilation has to be introduced. As a result, the expression for the air mass flow rate into the system, m_a, is expressed as

$$m_a = m_{nv} + m_{fv} \tag{4.21}$$

where m_{fv} is the air mass flow contributed by forced ventilation, and m_{nv} is the contribution from natural ventilation.

The natural ventilation rate through a vertical opening, m_{nv}, has been approximated by [34] to be proportional to the area of the vertical opening, A_{op_v} times the square root of the height of the opening, H_{op_v}.

$$m_{nv} = c_r A_{op_v} \sqrt{H_{op_v}} \tag{4.22}$$

The constant c_r was calculated by [34] to values ranging between 0.4-0.61 kg/s·m$^{5/2}$, and the value used here is $c_r = 0.5$.

It is assumed that any horizontal (roof) ventilation openings will serve as an exhaust only, meaning no air will enter the system through horizontal openings to add to m_{nv}.

The forced ventilation air mass flow rate is kept equal to m_a in the under ventilated model, namely

$$m_{fv} = m_f = 0.02u \tag{4.23}$$

4.3.3 Heat release rate, Q_C

Another notable adjustment that has to be made to the under ventilated model is the heat release rate Q_C. In the under ventilated case Q_C is limited by the air entering the system. Conversely, in the over ventilated case Q_C is limited by the propane entering the system. Q_C is therefore in the over ventilated case expressed as

$$Q_C = k_p \Delta H_p \tag{4.24}$$

where ΔH_p is the heat of combustion of propane and k_p a scaling constant to fit the theoretical model to the measurement data.

Note that the relation to m_p has been excluded. This is due to the fact that the maximum temperature in the system does not seem to be affected when m_p is increased, see Appendix C for measurement data from the over ventilated tests.

During over ventilated tests, it can be observed that the propane burns with a yellow flame and rarely produces any black smoke. This indicates that the governing combustion in the rig is given by the chemical equation

$$C_3H_8 + \frac{7}{2}O_2 \longrightarrow 3CO + 4H_2O \tag{4.25}$$

The heat of combustion of this reaction is $\Delta H_p = 1195,1$ kj/mol $= 27100$ kJ/kg.

4.3.4 Complete model

With the changes from the under ventilated model, the over ventilated model is fully expressed as:

$$\dot{T} = \frac{T}{c_p \rho_\infty T_\infty V}(Q_C - Q_W - Q_R) - \frac{T}{\rho_\infty T_\infty V}(m_a + m_p)(T - T_\infty) \tag{4.26}$$

$$\dot{T}_W = k_W(T - T_W) \tag{4.27}$$

$$Q_C = k_p \Delta H_p \tag{4.28}$$

$$Q_W = \varepsilon_W \sigma A_W (T^4 - T_W^4) + \alpha_W A_W (T - T_W) \tag{4.29}$$

$$Q_R = \sigma A_{op}(T^4 - T_W^4) \tag{4.30}$$

$$A_{op} = A_{op_v} + A_{op_h} \tag{4.31}$$

$$m_a = m_{nv} + m_{fv} \tag{4.32}$$

$$m_{nv} = c_r A_{op_v} \sqrt{H_{op_v}} \tag{4.33}$$

$$m_{fv} = m_f = 0.02u \tag{4.34}$$

4.3.5 Model verification

The over ventilated model was verified by comparing its response to measurement data from the tests conducted between May 12$^{\text{th}}$ and July 1$^{\text{st}}$ 2016. The constants k_w and k_p were tuned differently to fit each data set, and the values used is given in Table 4.1. The results of simulation is seen in Figures 4.7 - 4.11.

Table 4.1: List of parameters for the over ventilated model.

Test	k_w	k_p
12.05	0.030	0.36
28.06	0.025	0.66
29.06	0.025	0.68
30.06	0.025	0.62
01.07	0.035	0.39

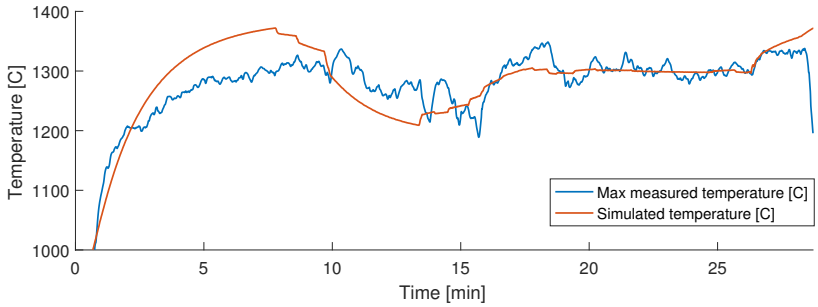

Figure 4.7: Measured max temperature and simulated temperature from 12.05.16.

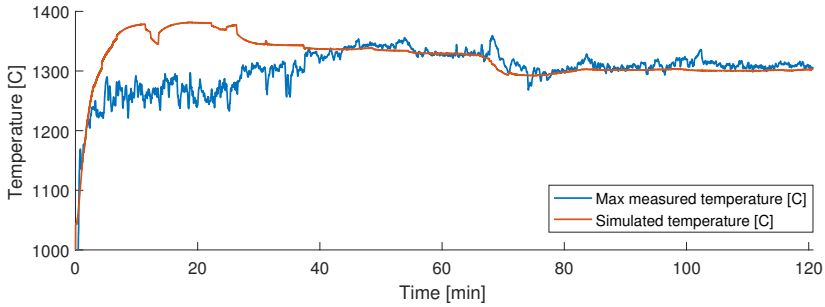

Figure 4.8: Measured max temperature and simulated temperature from 28.06.16.

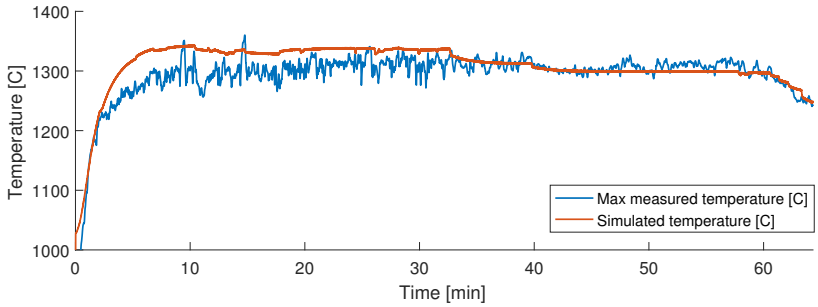

Figure 4.9: Measured max temperature and simulated temperature from 29.06.16.

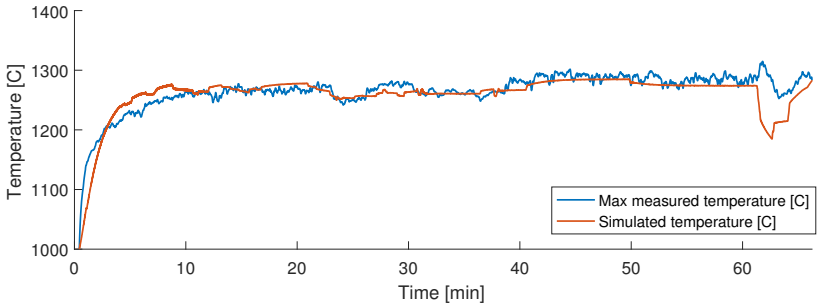

Figure 4.10: Measured max temperature and simulated temperature from 30.06.16.

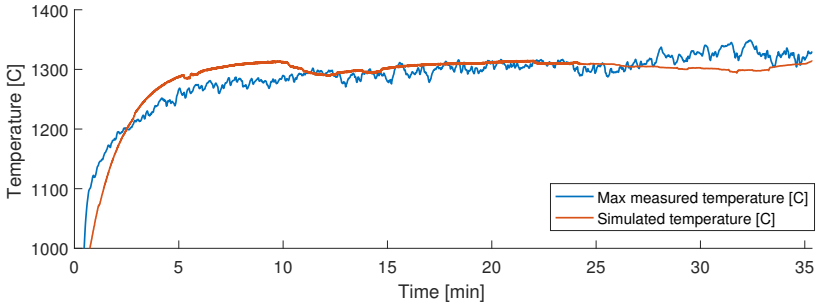

Figure 4.11: Measured max temperature and simulated temperature from 01.07.16.

4.4 Improving the over ventilated model

While the comparisons of measurement data to simulations of the over ventilated model are quite satisfactory, there is some room for improvement. After examining the test data closer, two new theories explaining the inaccuracies of the over ventilated model was developed and used create two new models: the mixed ventilated model and the modified over ventilated model.

4.5 Mixed ventilated model

The mixed ventilated model is largely based on the data from the test from 28.06.2016. In this test it can be seen that the maximum temperature increases as the fan input increases at low fan input, and decreases as the fan input increases at high fan inputs, see figure 4.12. This indicates that for lower fan inputs, the system is in the under ventilated state and needs help from the fans to supply sufficient oxygen for optimal combustion. At about $u = 40$ however, the system switches over to the over ventilated state, and further increased fan inputs will lead to temperature decrease. This theory motivates the need to merge the two models to create a mixed ventilated model, that automatically detects the state of the system and responds accordingly.

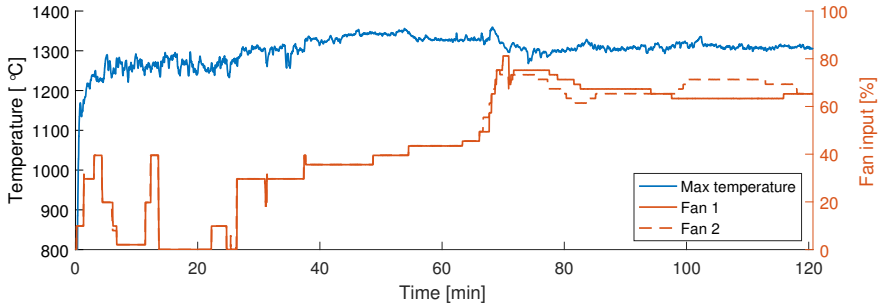

Figure 4.12: Fan input and temperature from 28.06.16.

4.5.1 Heat release rate, Q_C

To merge the two models, the over ventilated model was used as a basis because it includes the effect of natural ventilation. Aside from this, the only expression differing between the two models is the heat release rate, Q_C. These are therefore merged into one expression

$$Q_C = \begin{cases} k_a m_a \Delta H_a & , 0 < k_a m_a \Delta H_a < k_p \Delta H_p \quad \text{(Under ventilated state)} \\ k_p \Delta H_p & , k_a m_a \Delta H_a \geq k_p \Delta H_p \quad \text{(Over ventilated state)} \end{cases} \tag{4.35}$$

When the condition $k_a m_a \Delta H_a \geq k_p \Delta H_p$ holds, there is an excess of air in the system. The heat release rate is limited by the fuel, and the system is therefore in the over ventilated state.

4.5.2 Model verification

Just as the over ventilated model, the mixed ventilated model was verified by comparing its response to measurement data from the tests conducted between May 12th and July 1st 2016. The same k_w as in the over ventilated simulation were used, but in some cases k_p had to be tweaked a little bit. Additionally, k_a had to be tuned. A list of the values of k_p and k_a used is given in Table 4.2. The results of simulation is seen in Figures 4.13 - 4.17. The yellow dashed line indicates the state of the system, 1 corresponding to the under ventilated state and 0 the over ventilated.

Table 4.2: List of parameters for the mixed ventilation model.

Test	k_a	k_p
12.05	0.74	0.36
28.06	0.61	0.67
29.06	0.64	0.68
30.06	0.64	0.62
01.07	0.71	0.45

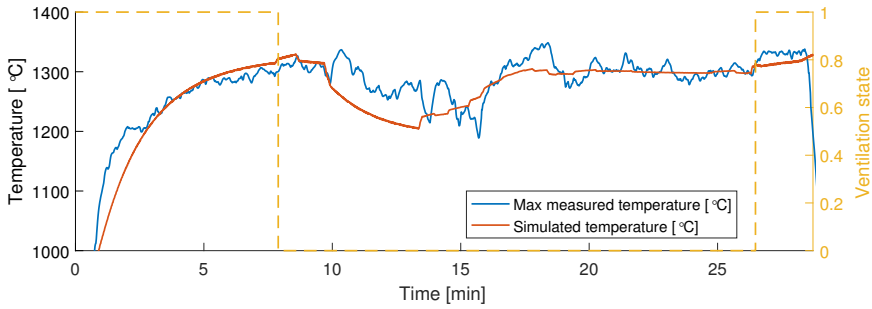

Figure 4.13: Measured max temperature and simulated temperature from 12.05.16.

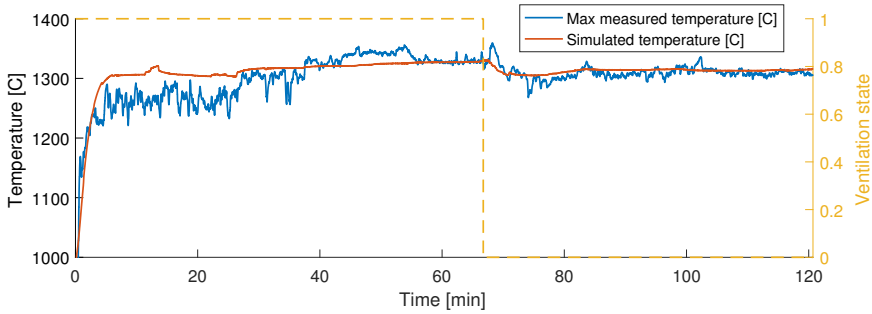

Figure 4.14: Measured max temperature and simulated temperature from 28.06.16.

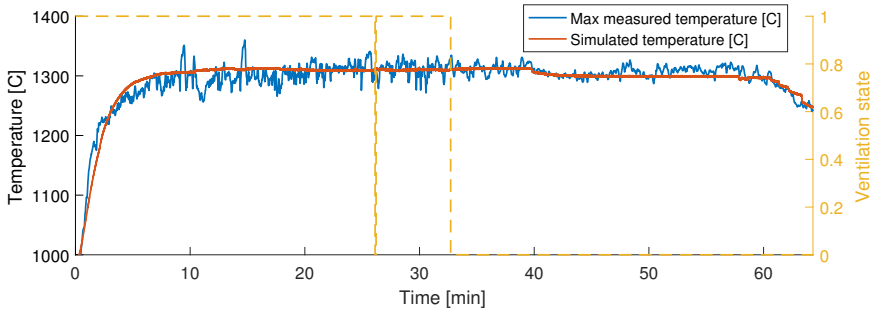

Figure 4.15: Measured max temperature and simulated temperature from 29.06.16.

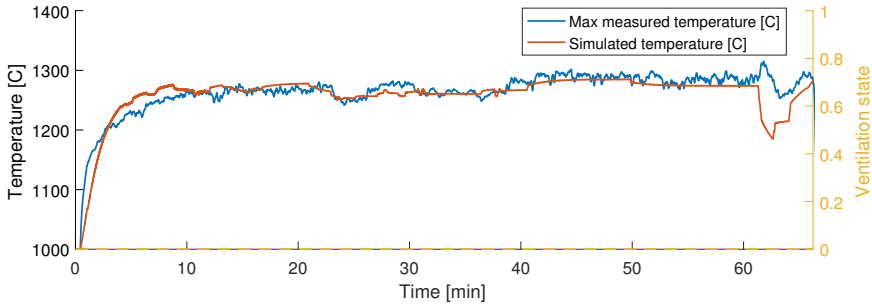

Figure 4.16: Measured max temperature and simulated temperature from 30.06.16.

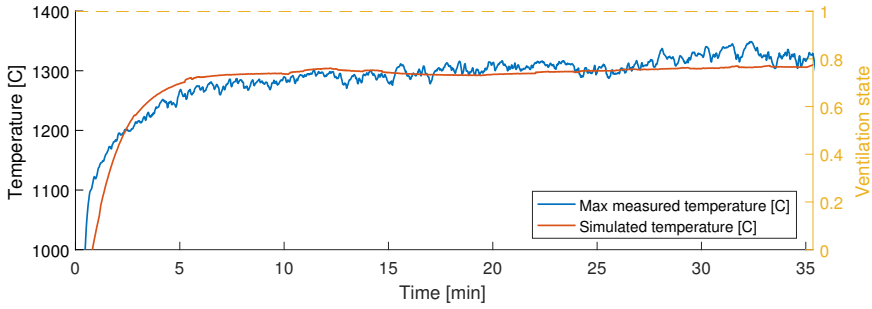

Figure 4.17: Measured max temperature and simulated temperature from 01.07.16.

4.6 Modified over ventilated model

While tuning the mixed ventilated model to match the data from 01.07.16, it was very hard to determine which of the two states the system was at at any given moment. This motivated another theory and consequently an additional model, the modified over ventilated model.

In the test from 01.07.16, the unactuated system struggled to reach the desired temperature of 1300°C, and when it finally did it was allowed to surpass this reference to even out the heat fluxes imposed on the test piece throughout the whole test. Because of this the fans were hardly actuated, and never exceeded $u = 20\%$. Moreover, these small fan inputs show no clear effect on the temperature of the system. In fact the fan inputs doesn't seem to affect the temperature at all, see figure 4.18. Thus the basis for a new theory explaining the systems dynamics was developed.

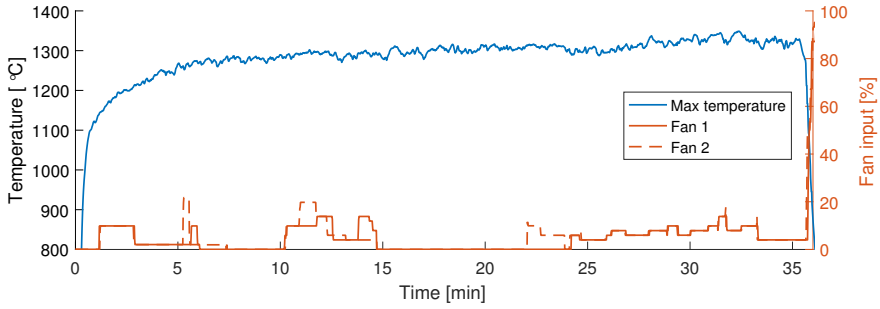

Figure 4.18: Fan input and temperature from 01.07.16.

This new theory supposes that low fan inputs does not affect the temperature of the system because the forced ventilation limits the natural ventilation. That is to say, when the fans are off the oven draws enough air naturally for the fuel to completely combust. When the fans are actuated, the oven does not need to draw as much air naturally and the rate of natural ventilation is decreased in unison with the increase in forced ventilation. The net air mass flow rate into the system is therefore unaffected by small fan inputs. When the fan input is sufficiently big, the mass flow rate through the system becomes large enough for the temperature to drop because of increased temperature loss.

4.6.1 Air mass flow rates supplied by fans

The over ventilated model can be easily adjusted according to the theory above by including a deadzone in the expression for the air mass flow rate supplied by the fans, m_f:

$$m_f = \begin{cases} 0.02u - dz_{lim} & , \quad 0.02u - dz_{lim} > 0 \\ 0 & , \quad \text{else} \end{cases} \tag{4.36}$$

4.6.2 Model verification

Figures 4.19 to 4.23 shows the results of simulation with deadzone implemented. k_p had to be retuned in each data set, but k_w was kept the same. A list of the values of k_p and dz_{lim} used is given in Table 4.3.

Table 4.3: List of parameters for the mixed ventilated model.

Test	dz_{lim}	k_p
12.05	0.4	0.33
28.06	0.4	0.63
29.06	0.4	0.64
30.06	0.2	0.62
01.07	0.4	0.39

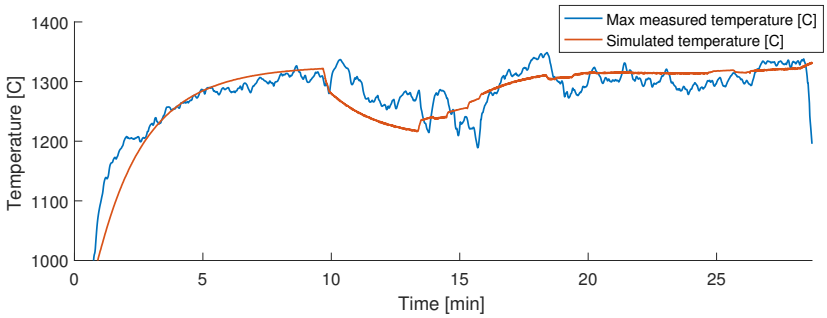

Figure 4.19: Measured max temperature and simulated temperature from 12.05.16.

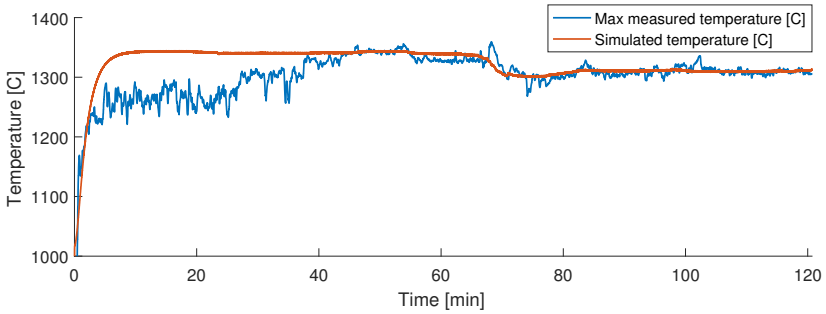

Figure 4.20: Measured max temperature and simulated temperature from 28.06.16.

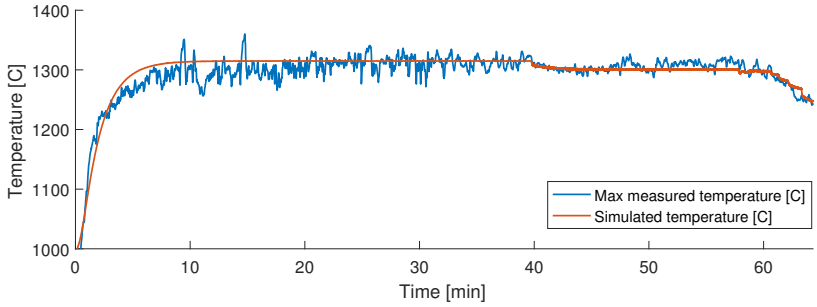

Figure 4.21: Measured max temperature and simulated temperature from 29.06.16.

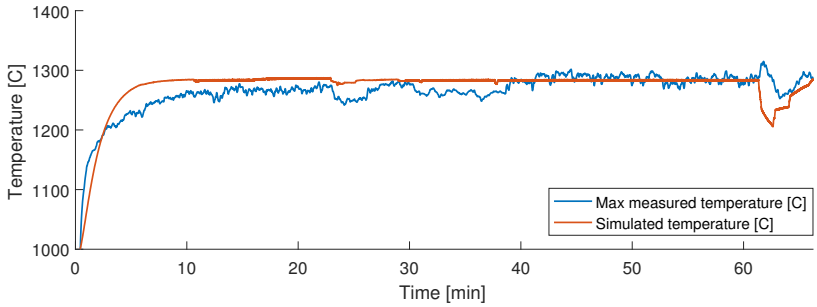

Figure 4.22: Measured max temperature and simulated temperature from 30.06.16.

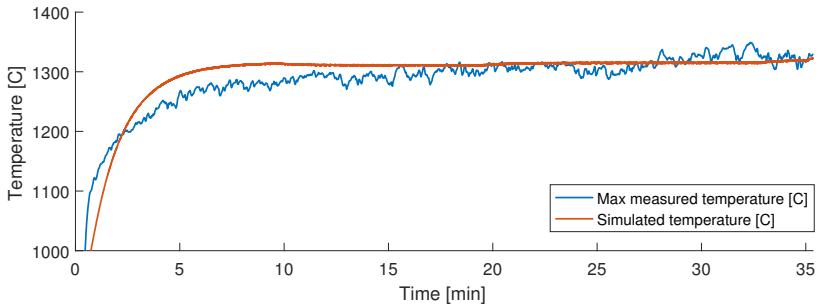

Figure 4.23: Measured max temperature and simulated temperature from 01.07.16.

Chapter 5

Temperature control

The main objective of this thesis is to automatically control the temperature of the over ventilated system. With a variety of mathematical models able to predict the systems temperature response, these can be utilized to create controllers and test their effectiveness through simulations. Out of the four existing mathematical models, the mixed ventilated model is not only the most accurate, but it also raises an interesting control problem. The dynamic of under ventilated response at low fan inputs and over ventilated response at higher fan inputs could be problematic. This is why the mixed ventilated model was chosen as the model used in the control simulations in this chapter.

The steady state responses of the mixed ventilated model without actuation reaches a temperature adequately close to the reference temperature for all parameter configurations used in the previous chapter. This makes the systems reaction to control laws slightly hard to analyze. The models response suggests that no assistance from the fans is needed at all. Despite this, the different control schemes were implemented to evaluate their effectiveness. To achieve a response as substantial as possible, the system was tuned as in the test from 12.05.16, which has the biggest deviation from 1300 °C when it is not actuated ($T_{steady}(u = 0) = 1308°\text{C}$).

Results of controlling the under ventilated model with PI control is included at the end of the chapter. These results are taken from the project thesis[35], where the main objective was to analyze the under ventilated systems response to control. These results were included because of the objective of comparing the two systems in this master thesis.

5.1 PID temperature control

The mixed ventilated system poses a curious problem concerning PID control; how should the error e, the input to the controller, be defined? In the under ventilated state, an increase in u increases the temperature in the system, and thus e should be defined $e = T_{ref} - T$. In the over ventilated state however, the exact opposite is true and e should therefore be

$e = T - T_{ref}$. As the system in this configuration is meant to be over ventilated, and the fact that a temperature somewhat lower than 1300°C is preferred over the opposite case, the latter definition for e is used. A simple implementation of PID control can be seen in figure 5.1. Note that as the process variable of the system is prone to be noisy, a noise signal v is added to the output of the plant before it is fed back to the controller.

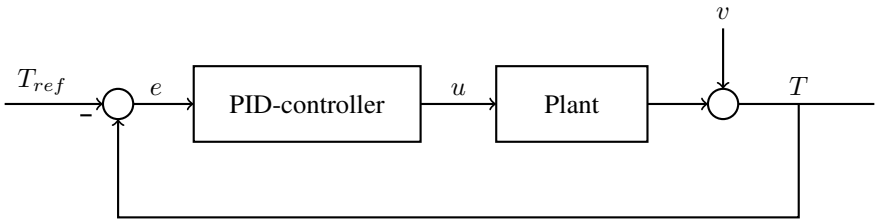

Figure 5.1: Block diagram PID controller with noisy signal fed back to the controller.

$$u(t) = K_c e(t) + \frac{K_c}{T_i} \int_0^t e(t)dt + \frac{K_c}{T_d} \dot{e}(t) \tag{5.1}$$

An implementation of the PID (Proportional, Integral, Derivative) control law is given in equation 5.1. In this expression, K_c is known as the proportional gain, T_i the integral action time, and T_d the derivative action time. In some cases however, a proportional band, PB is used in place of the proportional gain. When the input is unrestricted, the proportional band is calculated as in 5.2, and when it is restricted as in 5.3.

$$PB = \frac{1}{K_c} \cdot 100\% \tag{5.2}$$

$$PB = \frac{u_{max} - u_{min}}{K_c} \cdot 100\% \tag{5.3}$$

Note that the allowed input of the fans is restricted to values between $u_{min} = 0$ and $u_{max} = 1$, values of $u(t)$ calculated higher or lower is set to 0 or 1, respectively.

5.1.1 P control, sensitivity to noise

First, lets look at the simplest form of a PID controller, namely plain proportional (P) control with no integral or derivative action. At first glance, an implementation as simple as $u(t) = 50e(t)$ ($K_c = 50$, $T_i = \infty$, $T_d = \infty$) seems to work satisfyingly, see figure 5.2. However, this simple configuration is very sensitive to noise, which is prominent in the temperature measurements. Small temperature fluctuations will lead to large variations in u, see figure 5.3.

5.1.2 PI control, integral windup

When integral action is included, a different problem arises. Since the temperature starts so far from the reference, the effect of integral action grows so large that it limits the calculated input to never (or rather very slowly) reach the allowed workspace of the fans, see figure 5.4.

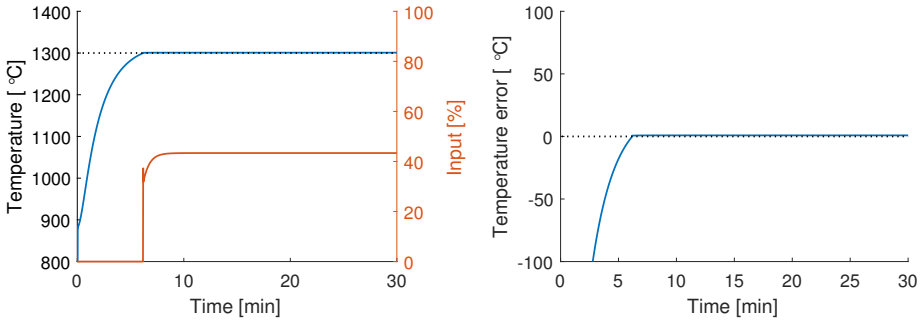

(a) Temperature response and control input.

(b) Temperature error, e.

Figure 5.2: System response to P control $K_c = 50$.

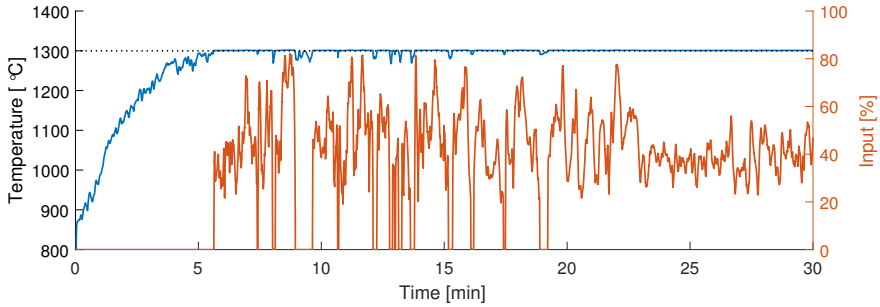

Figure 5.3: Systems response to P control with noise. $K_c = 50$.

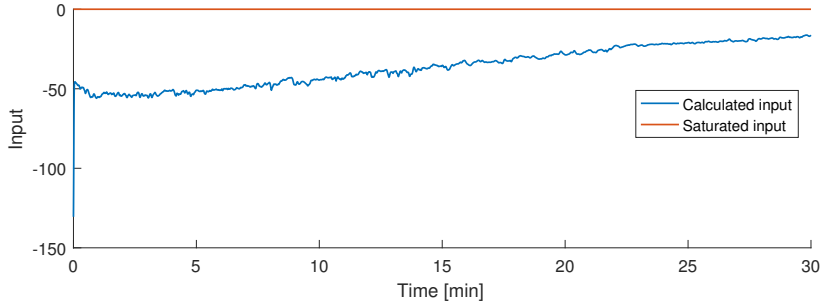

Figure 5.4: Example of integral windup. $K_c = 0.1$, $T_i = 100$.

5.1.3 PI control with limited integral action

A possible solution to the integral windup problem is to limit the integral action to only be in effect when the flame temperature is in vicinity of the reference value. By simulating different limits, the most effective scheme seems to be to omit integral action for all negative values of e. T_i is then expressed as

$$T_i = \begin{cases} 15 & , e \geq 0 \\ \infty & , e < 0 \end{cases} \tag{5.4}$$

The result of this modification is shown in figure 5.5. This modification solves the integral windup problem, but causes an undesired negative stationaty error. This is caused by the fact that the integral action is completely turned off when $e < 0$, which results in a P controller unable to sufficiently compensate for negative errors.

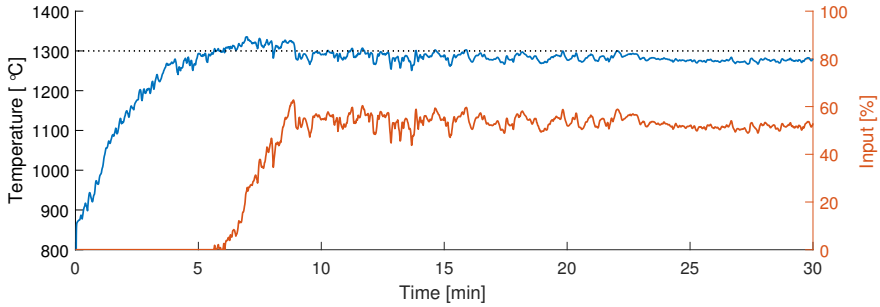

(a) Temperature response (blue) and control sequence (red).

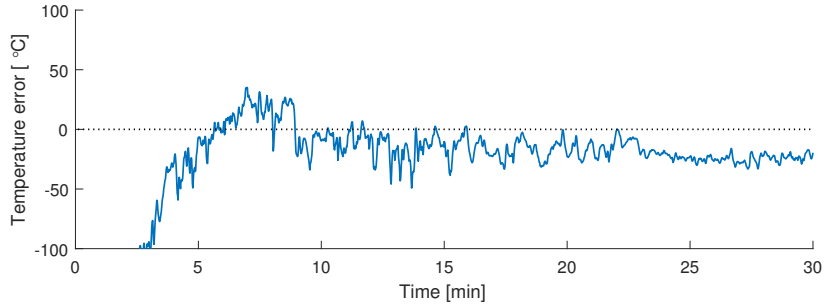

(b) Temperature error, e.

Figure 5.5: PI control with limited integral action, with noise. $K_c = 0.3$, $T_i = 15$, $T_d = \infty$.

5.1.4 PI control with clamping

To solve this problem, the integral action must remain on if the error should become negative after the initial transient. A solution to this is to implement hysteresis filtering. With hysteresis, the integral action turns on and off at different trip points depending on whether

the process variable is ascending or descending, as illustrated in figure 5.6. The same concept is used in the integral anti windup scheme called clamping, which is implemented in the Simulink PID block. This scheme simply turns off integral control when the control input is calculated outside of its limits. Results of simulating the system with PI control and clamping is shown in figure 5.7b

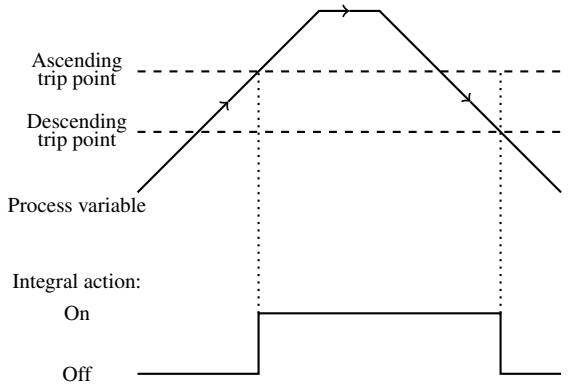

Figure 5.6: Hysteresis filtering to determine integral action

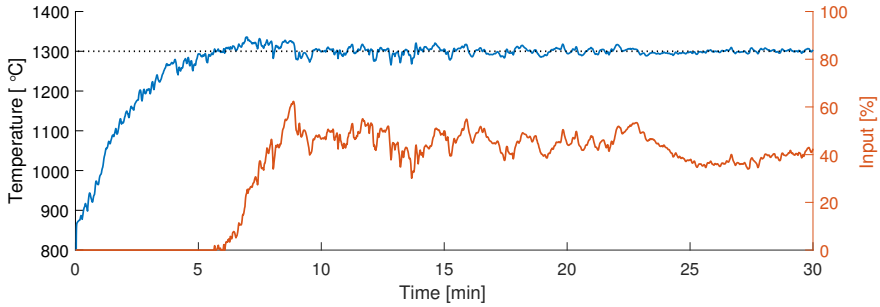

(a) Temperature response (blue) and control sequence (red).

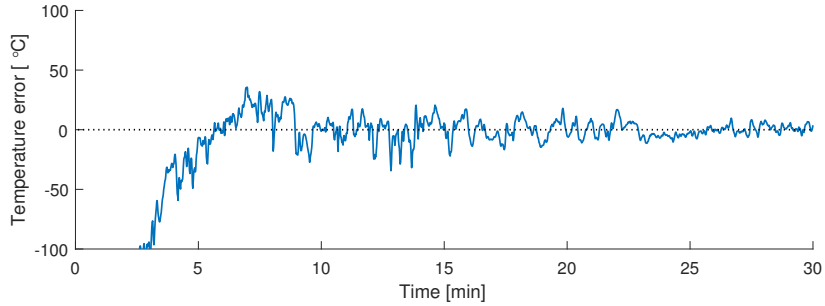

(b) Temperature error, e.

Figure 5.7: PI control with integral action limited by hysteresis, with noise. $K_c = 0.3$, $T_i = 15$, $T_d = \infty$.

5.1.5 PI control with back-calculation

Another integral anti windup scheme is back-calculation. This function is often integrated into PID blocks in programs such as MATLABs Simulink[1] and Labview[3]. This method uses a feedback loop to compensate for integral windup when the controller ”operates” outside of its limits. Simulinks implementation of PID control with back-calculation is illustrated in figure 5.8. Simulating the system with PI control and back-tracking with a back-calculation coefficient of $K_b = 0.1$ yields the same response as when clamping is used.

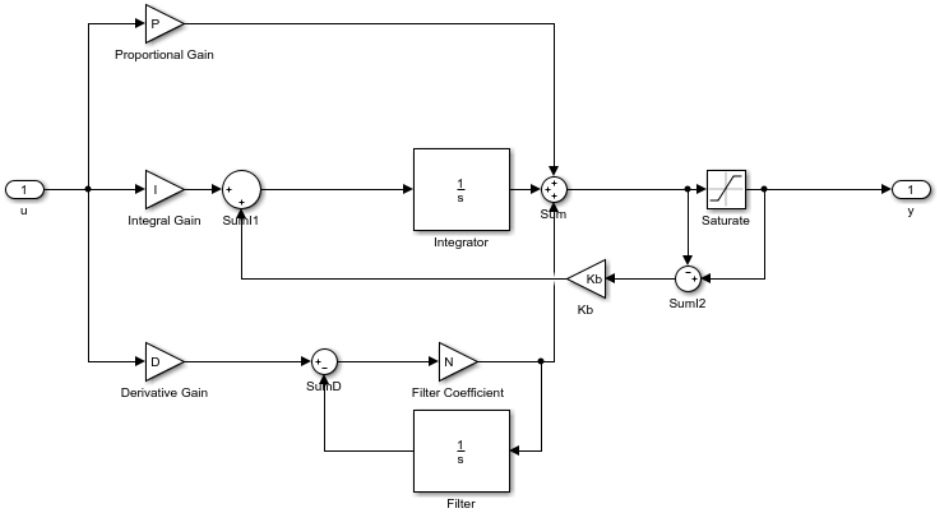

Figure 5.8: MATLAB Simulinks implementation of back-calculation[1].

5.1.6 PID control

Derivative action was tested, but quickly discarded as it does not have any positive effects on the control output. This is illustrated in figure 5.9.

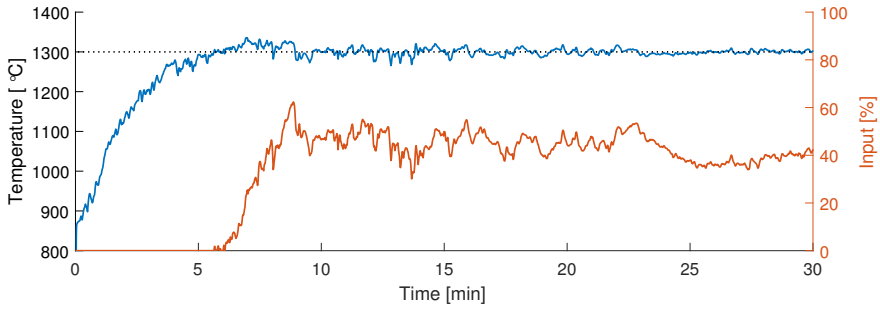

(a) $T_d = \infty$.

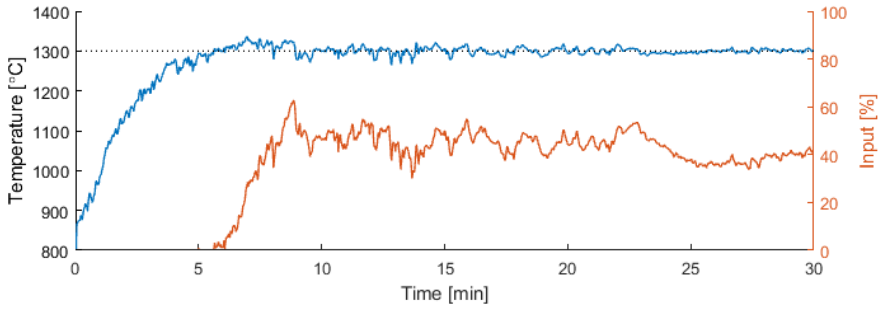

(b) $T_d = 10$.

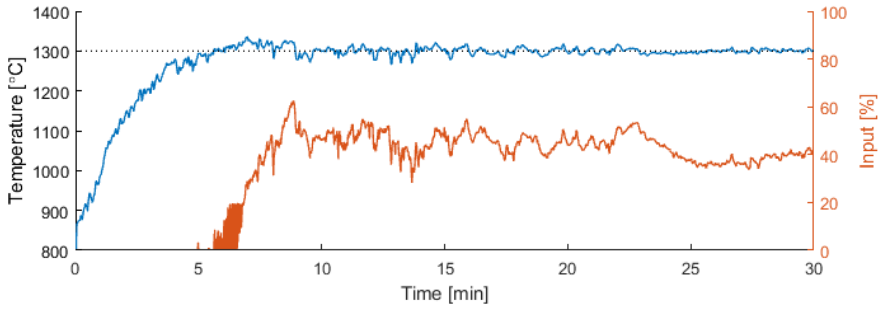

(c) $T_d = 1$.

Figure 5.9: Temperature response (blue) and control sequence (red) of PID control with different values of T_d. $K_c = 0.3$, $T_i = 15$.

5.2 MPC temperature control

Due to the limitations of the control input and the somewhat strict constraint of 1300°C, a Model Predictive Control (MPC) scheme is a natural choice for the system. An MPC controller uses a mathematical model to predict future states. It can therefore accommodate the control input to prevent the process variable(s) to exceed the established constraint(s). Mayne et. al. [19] describes the principle as

> *Model predictive control is a form of control in which the current control action is obtained by solving, at each sampling instant, a finite horizon open-loop optimal control problem, using the current state of the plant as the initial state; the optimization yields an optimal control sequence and the first control in this sequence is applied to the plant.*

The system with MPC control was simulated with measurement noise v similarly to the simulations with PID control. Figure 5.10 shows the block diagram of the implementation used in simulations.

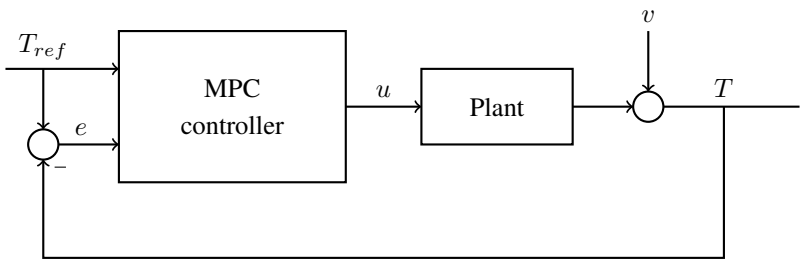

Figure 5.10: Block diagram MPC controller with noisy signal fed back to the controller.

Figure 5.11 shows the results of simulating the system with an MPC controller trimmed around the operating point of 1300°C, with constraints on the input u as before, and with a constraint of $T < 1300$°C. The MPC controller is more aggressive when the temperature constraint is surpassed, and so the temperature does not exceed 1300°C as much as with PI control.

A temperature constraint of 1350°C would be more fitting the systems requirements, but was not simulated as MPC control was ruled out. The added complexity and the small benefits of MPC compared to PI control made the latter option the most appealing, and PI proved to work satisfyingly when tested on the physical system.

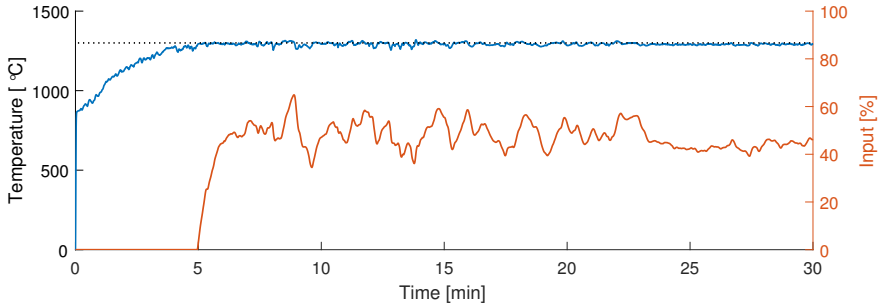

(a) Temperature response (blue) and control sequence (red).

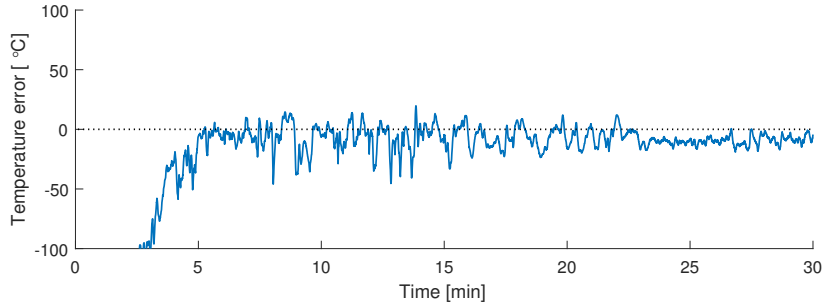

(b) Temperature error, e.

Figure 5.11: MPC control.

5.3 PI control of the under ventilated system

As mentioned in the chapter introduction, testing the under ventilated model for response to control was the objective of the project thesis. The results of PI control is included in this thesis on account of the objective to compare the two system configurations.

In the under ventilated system, increasing fan inputs will increase the temperature in the oven. The error fed into the PI controller is therefore expressed as

$$e = T_{ref} - T \tag{5.5}$$

This system has no problem with integral windup, so no integral anti windup scheme is needed. Other than these two factors the implementation of PI control is identical as in section 5.1. The PI parameters were tuned to $K_c = 0.5$ and $T_i = 250$. The results of simulation with these parameters and measurement noise is shown in figure 5.12. Since this system is prone to abrupt temperature drops the model does not include, PI control was also tested with a sudden temperature loss of 100°C at $t = 10$ min. The results are shown in figure 5.13

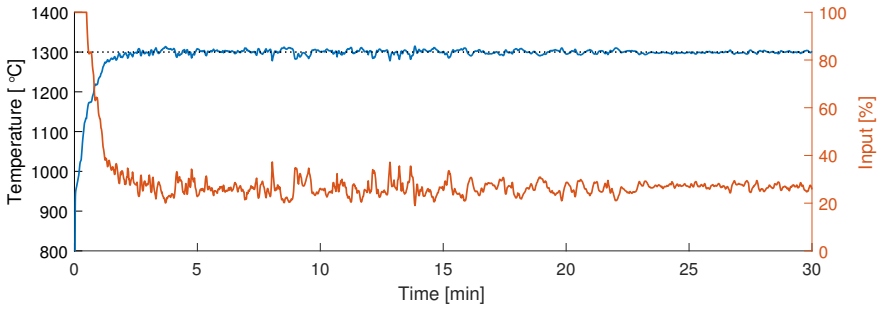

(a) Temperature response (blue) and control sequence (red).

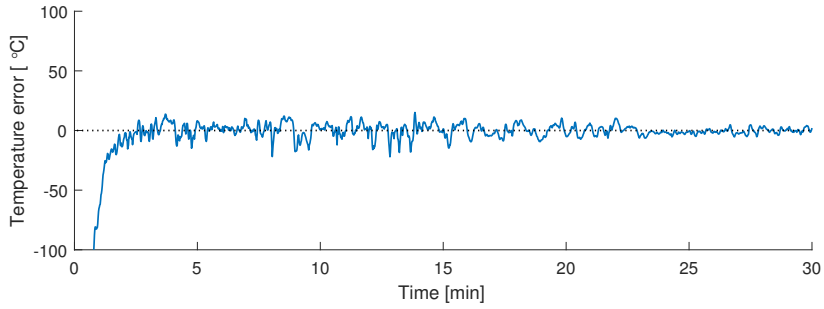

(b) Temperature error, e.

Figure 5.12: PI control of the under ventilated system. $K_c = 0.5$, $T_i = 250$.

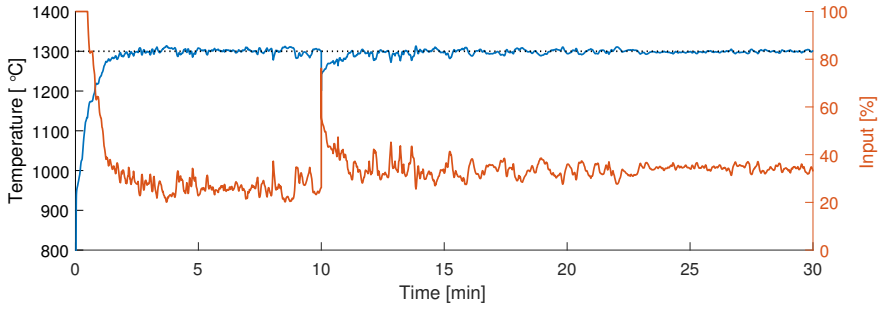

(a) Temperature response (blue) and control sequence (red).

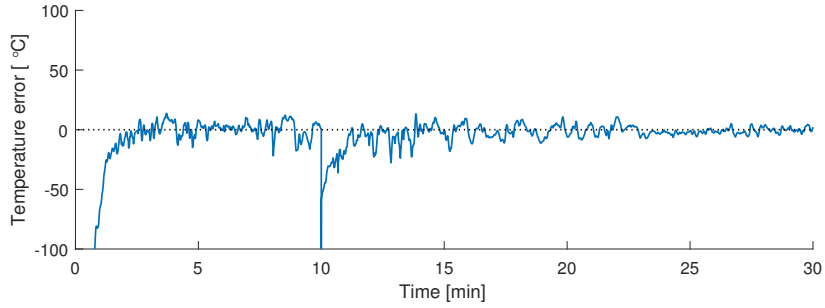

(b) Temperature error, e.

Figure 5.13: PI control of the under ventilated system, with simulated temperature drop at $t = 10$ min. $K_c = 0.5$, $T_i = 250$.

Chapter 6

Experiment

The simulations from chapter 5 suggest that PI control should work sufficiently well on the system. However, as the model neglects some of the dynamics of the system, it is important to conduct physical tests to validate the simulations predictions. Thus, tests with control were conducted on October 26th 2016. It was tested on the over ventilated system, as it is the main focus of this thesis. The purpose of this test was solely to verify that PI control is applicable on the process. Because of the relatively simple objective, the setup of the test was as easily done as possible, see figure 6.1. Two tests were conducted with different tuning parameters.

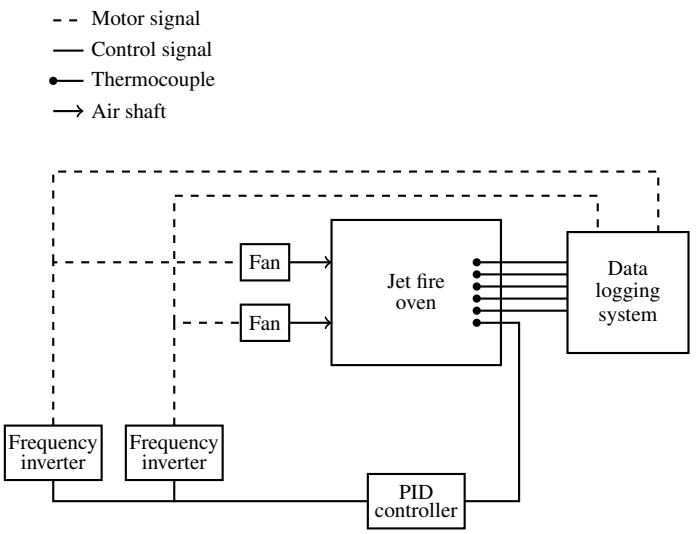

Figure 6.1: Setup of the experimental test.

6.1 Physical setup

The oven was built over ventilated, in the configuration with smaller ventilation openings described in section 3.5.2. This configuration was chosen as the data from the tests conducted in June 2016 suggested that the even more open option might struggle to reach the desired temperature of 1300°C.

The thermocouples were placed similarly to previous tests, with the middle row a little closer to the back wall.

6.2 Electrical setup

The controller used in these tests was an ABB Commander 350 [10]. It was used with a PID control template, with the setpoint locally chosen. The implementation of the control algorithm is completely unknown and the controller therefore somewhat of a black box. The ABB Commander seems to have both anti-integral windup and some sort of noise filtering implemented, making it very suitable to control the process.

Although the ABB commander 350 does support thermocouple inputs, the input was set to a 0 to 50 mV electrical range due to a missing cold junction part. The input was then scaled so that the process variable displayed and used by the controller was about a hundredth of the temperature measured by the thermocouple. That is to say, to regulate the temperature of the oven to 1300°C the set point of the controller was set to 13. Note by figure 6.1 that the thermocouple used to calculate this process variable was not otherwise recorded. The certainty of this scaling is therefore somewhat unclear, but for the purposes of this test it worked satisfyingly.

The output of the controller was a 0 - 20 mA current signal sent to the frequency inverters [6], each controlling their subsequent fan motors in compliance with the current input.

6.3 Tuning the controller

To verify the functionality of the controller settings, some testing was done prior to the rig experiments. This was done by heating a thermocouple with a gas burner and observing the control output. This way the functionality of the controller was discovered to be more advanced than presumed. There was no problem with integral windup or sensitivity to noise. The controller was thus tuned accordingly, not as originally planned. Notable parameters include the input filter time, set to 1, averaging the input values to produce a new input every second instead of updating the variable continuously. The ABB Commander uses proportional band to express the proportional portion of the PID control law, this was set to $PB = 500$. The integral action time was set to $T_i = 1$. Since derivative control action was deemed unnecessary by the simulations, the derivative action time was disabled.

6.4 Test 1

Figure 6.2 shows the control input and temperature measurements during the first test. At the red dashed line at about $t = 3$ min there was some water leakage into the oven, causing a temperature drop. It also caused two of the thermocouples to fail, and the measurement data from these are therefore omitted. Following this temperature drop it was decided to adjust the set point to 11 (about 1100°C) to study the controllers response. The set point was adjusted at about 5 minutes, where it can be seen the fans are turned on. At about ten minutes the set point was increased to 12, and again after 15 minutes to 13. The set point was lowered in the same manner towards the end of the test, as can be seen in figure 6.2.

Even though the controller works quite satisfactory, it is clear that it could be tuned better. With the lower set points, periodic temperature fluctuations occur suggesting the system is underdamped. When the set point was set to 13, the response is much more satisfying, but there are still signs of underdamped behaviour. The controller was therefore re-tuned before the second test to $PB = 800$ and $T_i = 5$.

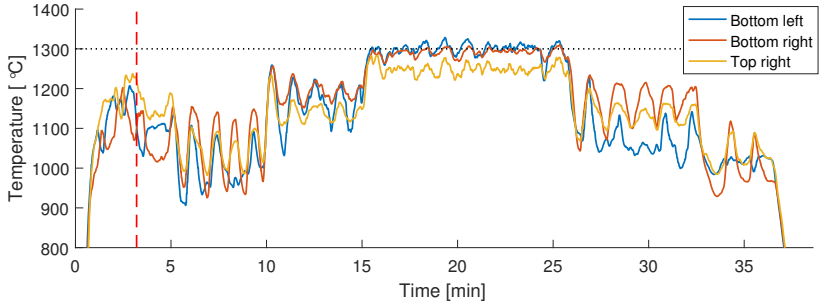

(a) Temperature measurements.

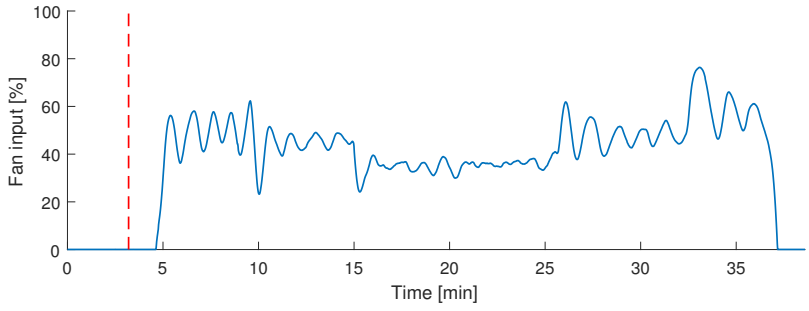

(b) Fan input control sequence.

Figure 6.2: Temperature measurements and control input during the first PI controlled test 26.10.2016. $PB = 500$, $T_i = 1$.

6.5 Test 2

Figure 6.3 shows the control input and temperature measurements during the second test. This test was conducted about 30 minutes after the first test. The walls of the oven could therefore be assumed to be completely dry, and the oven still held a temperature of about 50°C. As the goal temperature of 1300°C was easily reached in the previous test, it came as somewhat of a surprise that in this test the system struggled to reach the desired temperature. Ideally, 1300° should be reached in 5 minutes or less, but in this test the system needed about 10 minutes. The thermocouple fed to the controller held a temperature somewhat lower than the maximum temperature in the bottom right thermocouple, causing the controller to kick in even later and controlling the maximum temperature to about 1320°. Thus the temperatures observed over the reference value does not mean that PI control was unsuccessfull.

About 25 minutes into the test, the setpoint of the controller was reduced to 12, and later to 11 at 30 minutes. This was done to test the damping of the controller, which was greatly improved from the previous test, as can be seen in figure 6.3.

The two red dashed lines in figure 6.3 represents a time interval where the thermocouples were pulled closer to the oven walls. The setpoint was shortly after increased back up to 13. After the second red dashed line, the thermocouples were pushed back to their original positions.

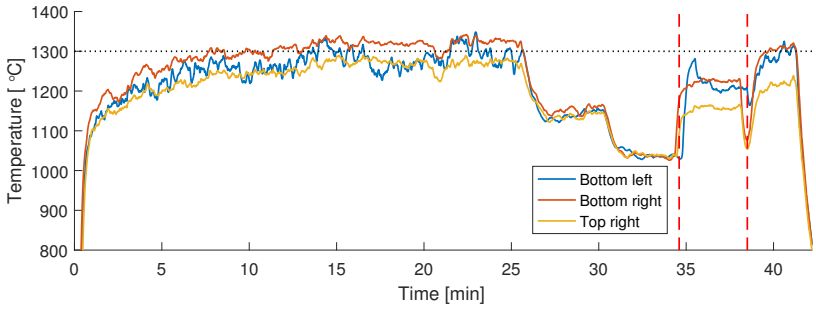

(a) Temperature measurements.

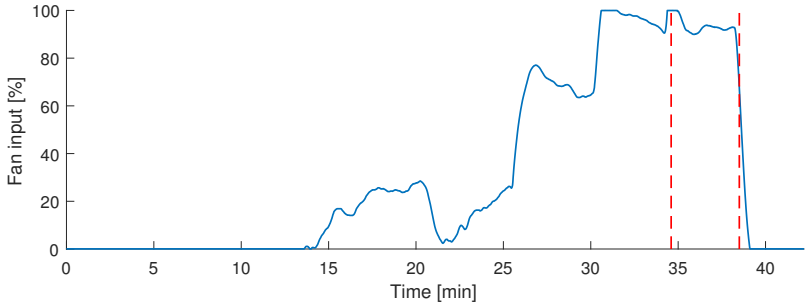

(b) Fan input control sequence.

Figure 6.3: Temperature measurements and control input during the second PI controlled test 26.10.2016. $PB = 800$, $T_i = 5$.

Chapter 7

Reference control

The motivation behind the temperature control is to ensure the test object has been exposed to the requested heat fluxes. The goal is that the heat flux averages a value of 350 W/m^2 at the end of the test. The running average of the heat flux is therefore calculated. The first five minutes is omitted from this calculation as the oven needs some time to reach high sufficiently high temperatures.

In many cases the over ventilated system has needed more than five minutes to heat to 1300°C. When this has happened, the reference value of the temperature has been set higher than 1300°C to increase the heat flux running average so that it reaches its goal by the end of the test.

The current proposed control scheme does not take this into consideration. An additional controller has to be implemented to adjust the reference temperature T_{ref} fed into the temperature controller. Since T_{ref} has a default value of 1300°C, the control output should regulate T_{ref} in an area around this point. T_{ref} is therefore expressed as

$$T_{ref} = 1300 + u_r \tag{7.1}$$

In simulations, the heat flux running average was estimated using the calculated value of T. A simple estimate of $\phi = T - 950$ was used as it provides a satisfying result in the relevant region. The running average of this estimate is then continuously updated after five minutes. The block diagram for the system simulated with reference control is shown in figure 7.1.

To properly test the reference controller, an additional temperature loss was added to the initial transient of the temperature plant, simulating cases where the oven needs more time to reach the desired 1300°C. The PI controlled temperature response of this modified plant is shown in figure 7.2, as well as the plot of the heat flux and its running average (starting at $t = 5$ min). The same PI control is used in all subsequent simulations. As seen in figure 7.2b, ϕ_{avg} does not quite reach the desired 350 kW/m^2.

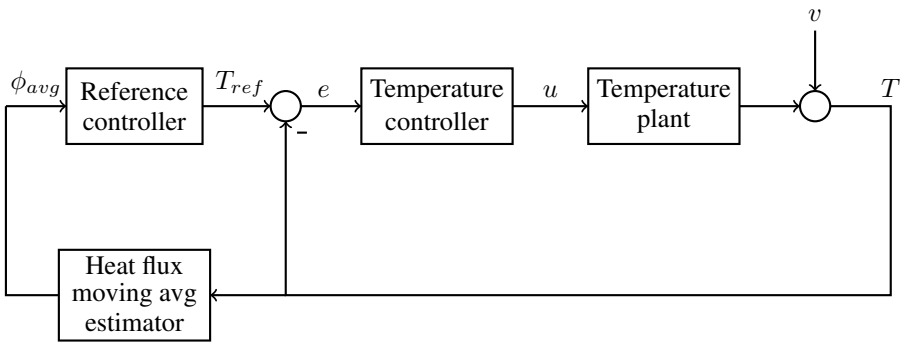

Figure 7.1: Block diagram of temperature and reference control simulation.

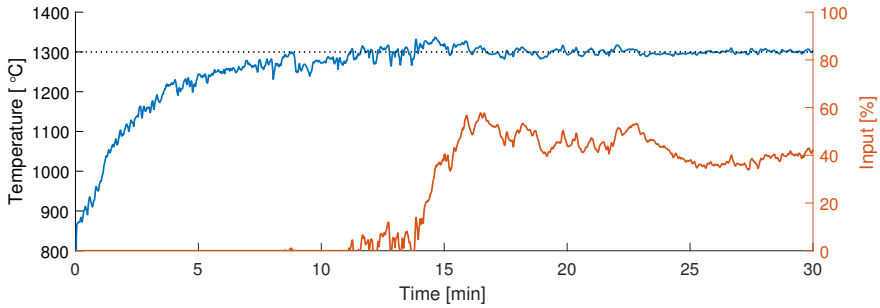

(a) Temperature response (blue) to PI controlled input (red).

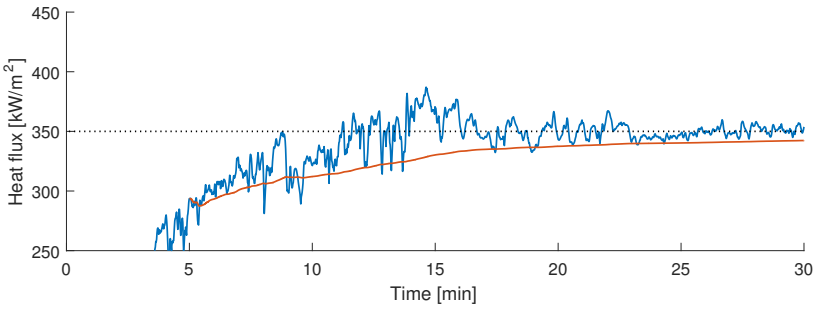

(b) Heat flux (blue) and its running average (red) starting at $t = 300$.

Figure 7.2: Temperature and heat flux response of PI controlled system with initial transient temperature penalty.

7.1 Proportional reference control

When the heat flux running average lies below the desired 350 kW/m^2, it is evident that the temperature reference, T_{ref}, has to be set to a higher value. Since the running average is a smooth, practically noiseless signal, a control scheme as simple as proportional control should suffice. Since temperatures around 1350°C are very undesirable, T_{ref} should be limited to values lower than 1330°C. The expression then becomes

$$u_r = \begin{cases} k_{rp}e_\phi & k_{rp}e_\phi < 30 \\ 30 & k_{rp}e_\phi \geq 30 \end{cases} \tag{7.2}$$

with k_{rp} being the reference control proportionality constant, and e_ϕ the error of the heat flux running average

$$e_\phi = \phi_{ref} - \phi_{avg} \tag{7.3}$$

The results of simulation with proportional reference control is given in figure 7.3. The reference proportionality constant used is $k_{rp} = 2$.

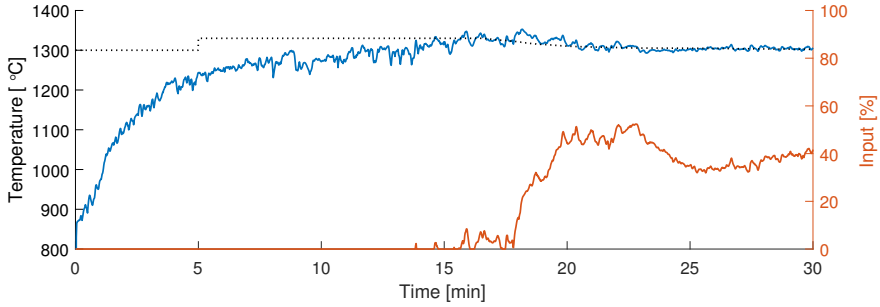

(a) Temperature response (blue) to PI controlled input (red). The black dotted line indicates the reference temperature.

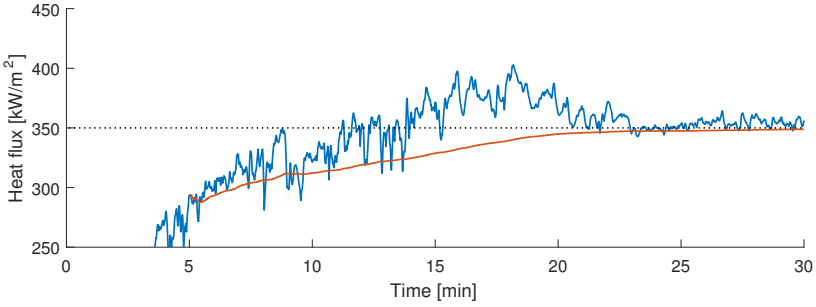

(b) Heat flux (blue) and its running average (red) starting at $t = 300$.

Figure 7.3: Temperature and heat flux response of P controlled reference control with initial transient temperature penalty. $k_{rp} = 2$.

The nature of the P controller (stationary error) causes T_{ref} to lie a bit above 1300°C towards the end of the test. However, this is not an undesirable outcome and can therefore be safely overlooked.

7.2 Step reference control

Another possible reference control implementation is a step controller. This controller adjusts u_r up or down when e_ϕ is large. When e_ϕ is sufficiently small, u_r is set to 0. An implementation is thus given by

$$u_r = \begin{cases} 30 & e_\phi < -5 \\ 0 & -5 \leq e_\phi \leq 5 \\ -30 & e_\phi > 5 \end{cases} \tag{7.4}$$

and the response of the system simulated with this controller is seen in figure 7.4.

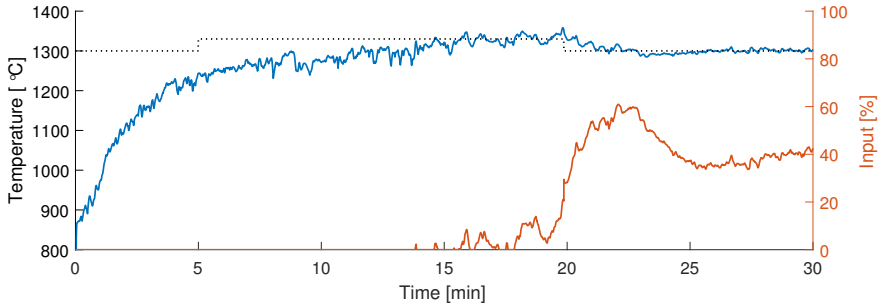

(a) Temperature response (blue) to PI controlled input (red). The black dotted line indicates the reference temperature.

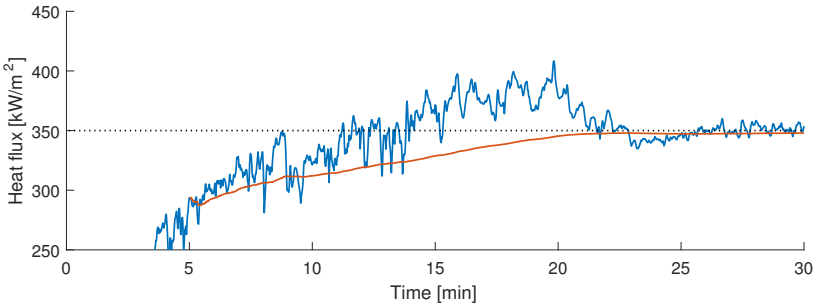

(b) Heat flux (blue) and its running average (red) starting at $t = 5$ minutes.

Figure 7.4: Temperature and heat flux response of step controlled reference control with initial transient temperature penalty.

Because of the sudden change in T_{ref}, the temperature error e experiences a sudden increase, prompting the temperature controller to react more forcibly than with a P reference controller.

Chapter 8

Fault detection in thermocouples

During the duration of a test, the possibility of a fault in one or more of the thermocouples is considerable. If this occurs, the faulty measurements can have a negative effect on the process variable used to calculate the control input. Implementing an algorithm that automatically detects and terminates faulty thermocouples would therefore greatly benefit the automation process.

This chapter describes how thermocouples work and how they can produce erroneous data. Examples of erroneous data from previous tests are presented and analyzed to propose a way to automatically recognize faulty data.

8.1 How thermocouples work

Thermocouples utilize the Seebeck effect to measure temperature[4]. The thermocouple consist of two wires of different metals. These two wires join at one end, the point where the temperature is measured. This is called the hot junction. The other end of the wires forms the cold junction. The Seebeck effect creates a voltage difference between the hot and the cold junction. Because of the differing metals and therefore properties of the two wires, the voltage at the cold junction is not the same for the for both wires. The voltage difference at the cold junction can therefore be measured and used to determine the temperature at the hot junction. The thermocouple is illustrated in figure 8.1.

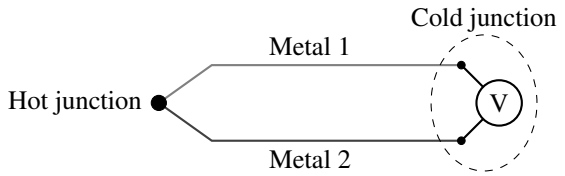

Figure 8.1: Thermocouple.

8.2 Errors in measurement from thermocouples

The voltage difference measured in the cold junction is small, in the millivolt range. Thermocouple measurements are therefore sensitive to noise and measurement gain and offset errors[31]. The most frequent source for erroneous measurements in the oven is however due to circuit shorting[7]. Any shorting of the thermocouple wires will create a new junction, and the measured temperature will be that of the new junction, see figure 8.2.

Figure 8.2: Thermocouple.

In the available measurement data, several examples of erroneous measurements occur. Figure 8.3 displays a fault from the test on 22.10.15. The measurement data in the faulty thermocouple comes from a cubed measuring point. The thermocouple is contained within a 40x40x40mm steel cube at the end of a 8mm steel tube, resulting in a slower response and a smoother measurement up until the fault occurs. The fault appears as high frequency temperature fluctuations, and after the measurement resembles that of the ”free” thermocouples, such as the control. This indicates that the new junction after the fault lies somewhere in the steel tube.

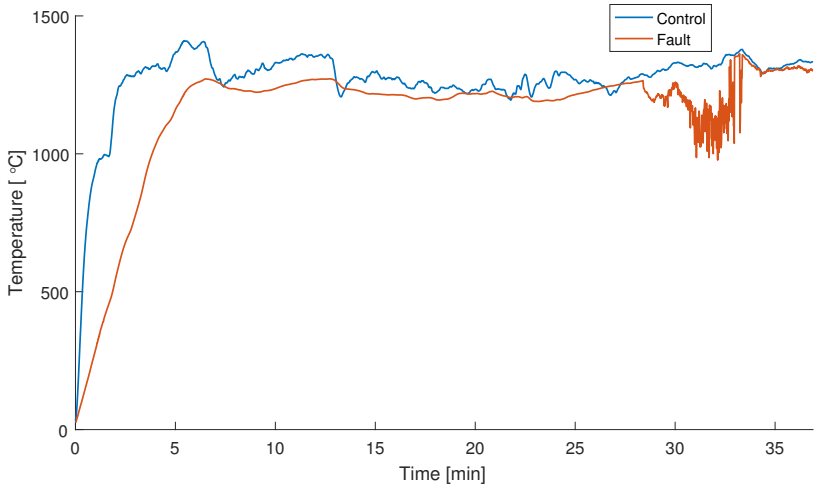

Figure 8.3: Measurement error in cubed thermocouple from 22.10.2015.

In the data from 12.05.16 and 26.10.16, figures 8.4 and 8.5 respectively, the same trend is seen in the faulty data. This data features very large temperature fluctuations, the measurement varying up to 700°C between single data points. This is likely due to the thermo-

couple shorting on and off further down the line. The trends in fault 2 in figure 8.5 where the the measurement decreases and settle at a low temperature, the new junction presumably moved down the thermocouple wires and settled in a point outside of the oven. The thermocouple responsible for fault 1 was manually pulled out of the oven.

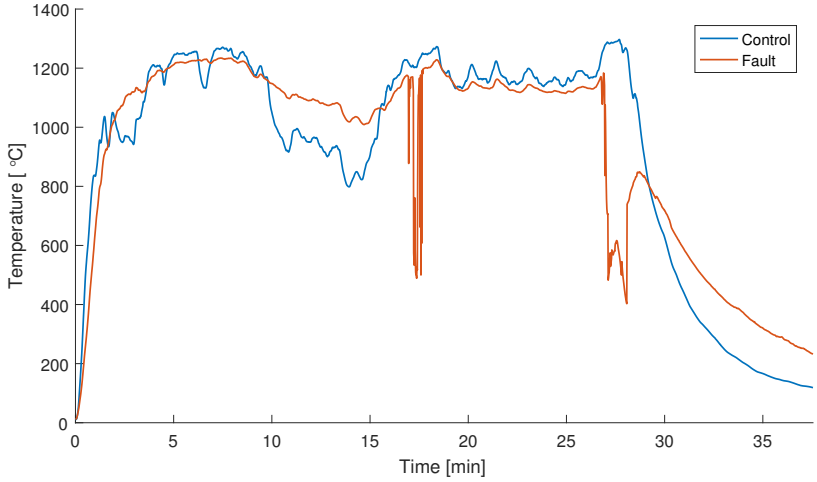

Figure 8.4: Measurement error from 12.05.2016.

8.2.1 Measurements from damaged thermocouples

Figure 8.6 shows data from the second test conducted on 26.10.2016. The faulty thermocouple is the same as the thermocouple responsible for fault 2 in the previous test, see figure 8.5. The data obtained from this thermocouple clearly has vaster noise than the control. This indicates that a thermocouple that has previously failed is not reliable and should be terminated.

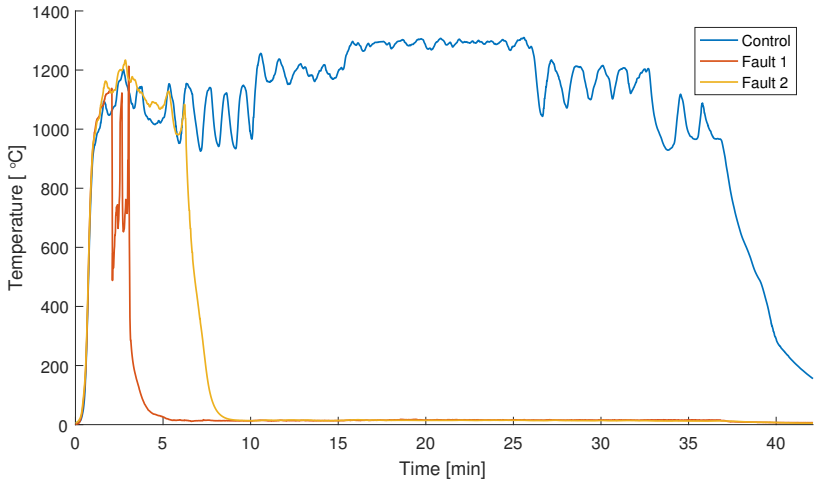

Figure 8.5: Measurement error from the first test 26.10.2016.

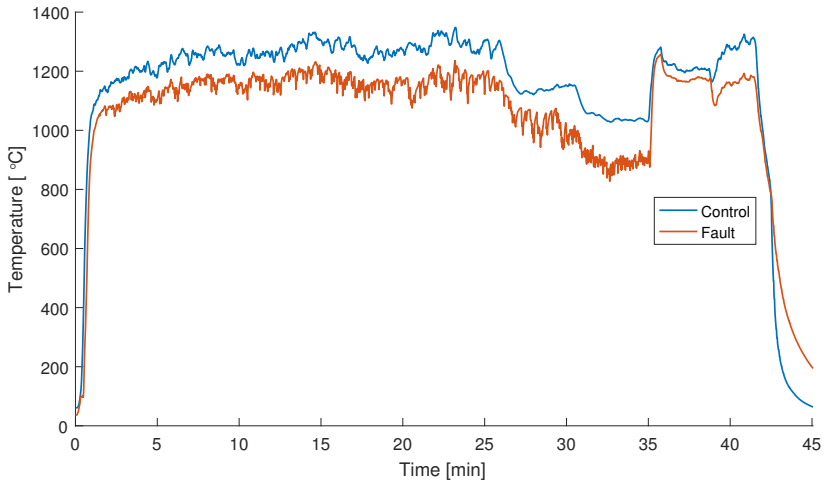

Figure 8.6: Measurement error from the second test 26.10.2016.

8.2.2 Thermocouples exposed to high temperatures

The thermocouples used to measure oven temperatures are mostly type K. These thermocouples can measure a temperature up to 1370°C. Although it is undesirable, higher temperatures may occur in the oven. This causes the thermocouples to fail. Two different consequences of too high temperatures are found in the available measurement data, shown in figure 8.7. In 8.7a the thermocouple temporarily stops logging when the temperature is too high. In 8.7b the thermocouple records 1370°C for a while before it stops recording entirely. Note that the control measurement in 8.7b is a platinum thermocouple capable of withstanding even higher temperatures.

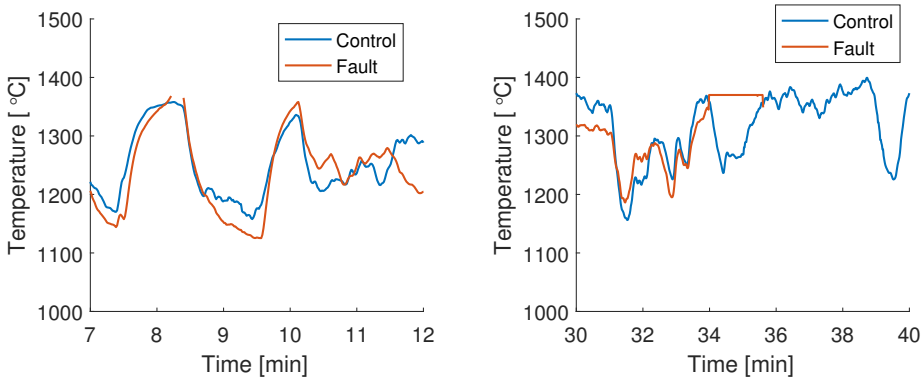

(a) Thermocouple stops logging, starts again when temperatures are within range.

(b) Thermocouple logs 1370°C and then stops logging.

Figure 8.7: Faults when thermocouples are exposed to high temperatures.

8.3 Fault detection

Fault in thermocouples reveals itself in many ways, and is not limited to the manifestations documented in the previous section. The principle of thermocouple shorting can produce erroneous data of any kind, depending on when and where the short happens, if it moves or if the wire fluctuates between shorted and unshorted states. This makes it harder to detect and isolate the faulty data, although not impossible. A lot of research has been done in the field of fault detection, and methods and hardware patents have been crated. The most promising methods are in the field of statistical processing, such as multiscale analysis[33], principal component analysis (PCA)[36], modified independent component analysis (ICA)[27] and canonical variate analysis[21].

The good new is that a thermocouple short will not produce any temperature measurements higher than the maximum temperature inside the oven. These faults will therefore not create any problems for the control algorithm, which utilizes the maximum temperature as its process variable.

Chapter 9

Discussion

In this chapter, some missing factors from the model is presented which provides possible explanations to model deviations. The advantages and disadvantages of the different builds are discussed to suggest what system is the most successful, and when.

9.1 Wall condition variables

In all the over ventilated tests, the oven reaches a temperature of 1200°C within a few minutes. However, the time it takes for the temperature to reach 1300°C varies largely from test to test. What determines this variable time delay is not included in the mathematical model and therefore unclear, but it is likely determined by the wall conditions.

The properties of the walls changes from test to test. Exposing the walls to high temperatures will slowly damage them and thus change their properties and the ovens ability to store energy. If the oven has been used in previous tests, the system will likely need more time to reach 1300°C than if the oven was freshly built.

Another variable wall factor is the moisture stored within the walls. This changes from test to test depending on weather conditions. If it has previously rained or it is raining during a test, there is likely water stored in the walls. The system will then use energy to evaporate the water stored in the walls, and thus lead to a slower temperature increase in the beginning of the test than if the walls were completely dry.

These factors are somewhat represented in the wall temperature coefficient k_w, but this is too simple an implementation to obtain an accurate model response. The simulated temperature is therefore usually higher than the measured temperature in the first 10-20 minutes of the test comparisons, see sections 4.3.5 and 4.5.2.

9.2 Temperature gradient neglected by the model

If the reasoning behind the modified over ventilated model is correct and the system is unaffected by small fan inputs, another phenomenon is clearly visible in the temperature data from 01.07.16. After the initial transient, there is a clear temperature gradient throughout the experiment, as shown in figure 9.1. The temperature gradient $T_{\triangledown}$ illustrated in this figure estimates a temperature increase of 2°C per minute after the initial five minutes.

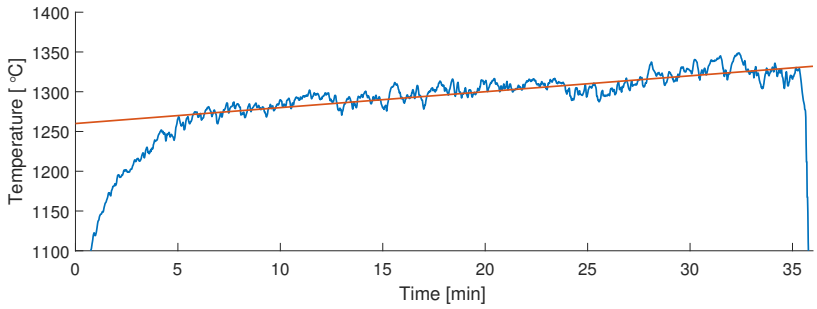

Figure 9.1: Maximum temperature (blue) and a linear approximation of the temperature gradient from $t = 5$ min (red). $T_{\triangledown} = 1260 + 2t$.

Although less clear, the same trend can be assumed to occur in all other tests, both over and under ventilated. This gives an explanation to why the simulations from the under ventilated tests tends to deviate negatively towards the end of the test. The ovens ability to store energy and therefore maintain the high temperatures increases with the duration of the test, causing the operating range of the system to shift, and therefore change the effect of the fans. The larger deviations in the under ventilated tests suggests that this temperature gradient is greater in the under ventilated system than the over ventilated. This is likely because the temperature gradient is also determined by the wall conditions. Since the wall surface area is greater in the under ventilated system than the over ventilated system, it also has a greater effect.

9.3 Effects of wind

In the over ventilated tests where weather measurements are available, there are considerable differences in the wind conditions. Both wind speed and bearing vary in the first three tests, hitting the oven from different sides. In the fourth test the wind conditions are very similar to the third, but the oven was built with smaller ventilation openings. The average wind speeds and bearings are given in table 9.1. Detailed time lapses of the wind conditions are found in appendix D. The oven is situated with the front facing about 150

Table 9.1: Average wind speed and bearing from over ventilated tests.

Test	Avg. wind speed	Avg. wind bearing
28.06	1.1 m/s	94°
29.06	3.4 m/s	15°
30.06	4.9 m/s	180°
01.07	4.3 m/s	185°

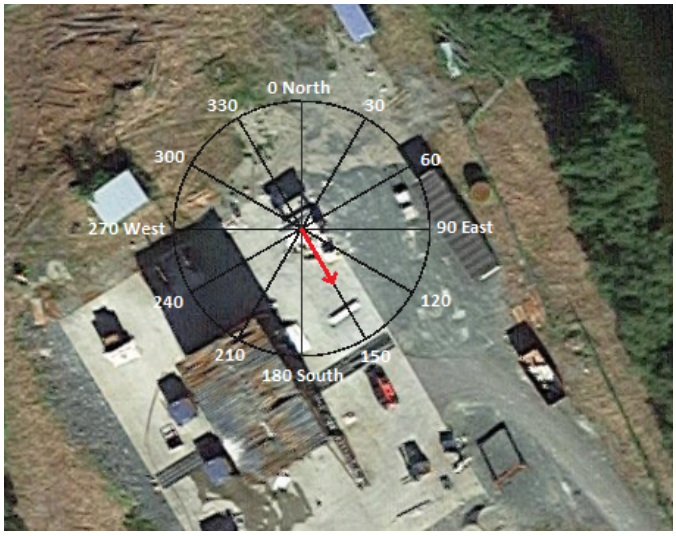

Figure 9.2: Areal view of the oven with orientation. The red arrow indicates the direction of the front opening of the oven, facing 150 degrees southeast. Source: Google Earth[2].

degrees southeast, as illustrated in figure 9.2. With this knowledge and the temperature data, the effects of wind can be discussed.

In the test from 28.06, the wind is weak compared to the other tests. This is also the test where the oven seems most clearly to be in the under ventilated state for low fan inputs. It is therefore possible that this system relies on substantial wind to draw enough oxygen to maintain the over ventilated state.

The best test results are those from 29.06. Here the wind speed is more substantial, but it is hitting the oven from the side and the back, where the ventilation openings are smaller.

The most interesting weather data is from the last two tests. Here, the wind is stronger and blows almost directly into the front of the oven. The possibility that this wind is what causes the temperatures in the oven to stay under 1300°C in the test from 30.06 is considerable. The following day, the oven was built with smaller openings, making it more robust and less affected by the wind. It is therefore advisable that on days with higher wind speeds and/or bearing towards the front of the oven, the front opening should be built a bit smaller.

While these observation are worth considering when building the oven, their validity has yet to be verified by further testing.

9.4 Effects of rain

As mentioned earlier, the ovens walls will store moisture. Rain prior to a test will therefore change the ovens properties as they contain water. In the available measurement data from previous tests (see appendix D for weather measurements), notable rains occurred prior to two tests: the under ventilated test 22.10.15 and the over ventilated test 28.06.16. In the under ventilated test, the rain has no obvious effect on the systems response. The over ventilated test featuring rain prior to the test is however one that struggles to reach the desired temperature of 1300°C. It is possible this is because of the moisture stored in the oven.

9.5 Under vs over ventilated systems

With the two options of over and under ventilated systems comes the question of which system is the better choice. The pros and cons of both systems is discussed in this section to provide insight into how the oven should be built for a specific test.

9.5.1 Controllability

The smaller the ventilation openings are, the more robust the system is expected to be. There are less uncontrollable input factors due to uncontrollable conditions, such as wind. The under ventilated system should therefore be expected to be more stable and controllable than the over ventilated system, but this seems not to be the case. Unforeseen temperature changes are more frequently experienced in the under ventilated system. This is emphasized by the mathematical models, the under ventilated simulations tends to stray from the measurement data more than the over ventilated simulations. However, not a lot of tests have been conducted in the over ventilated system, and the validity of this conclusion should be questioned. Because this system is more exposed to the elements it is likely more affected by the weather conditions. So far all tests have been conducted in nice summer weather, it should be expected to struggle more in harsher winter conditions.

The under ventilated system has a much bigger control region than the over ventilated, as can be seen by comparing data from the two different configurations. A small change the fan inputs has a big effect on the under ventilated system, while the over ventilated system requires a big increase in fan inputs to lower the temperature by a few degrees.

Although unexpected temperature changes in the under ventilated system are alarming, they have never been too big for the system to handle. The desired temperature of 1300°C has always been recoverable by adjusting the fan inputs. Although PI control has not been tested on the under ventilated system, it is expected to work just as well as in the over ventilated system.

9.5.2 Black smoke production

An undesirable factor in the tests is the production of black smoke. A lack of oxygen when the propane reacts leads to incomplete combustion. When very little oxygen is available, propane combusts by the chemical equation

$$C_3H_8 + 2O_2 \longrightarrow 4H_2O + 3C \tag{9.1}$$

The pure carbon (C) produced by this reaction creates the black smoke. Naturally, black smoke production is much more likely to occur in the under ventilated system, as the temperature is lowered by limiting oxygen in the system and thus increasing the rate of incomplete combustion. The over ventilated system is therefore more advantageous considering black smoke production.

9.5.3 Limitations in control region

When the fans are actuated in the under ventilated system, the temperature increases. Conversely, the temperature decreases when the fans are actuated in the over ventilated system. As the oven responds differently from test to test, these limitations become problematic when the unactuated system reaches too high or too low temperatures.

In some cases the under ventilated system has unexpectedly drawn enough air naturally to reach temperatures above 1300°C. The test from 14.04.2016 is an example of this, see figure B5 in Appendix B. When this happens, there is no way to purposefully reduce the temperature inside the oven, as increased fan inputs will only increase the temperature further.

The over ventilated system however risks too low temperatures, as in the test from 30.06.2016. If the unactuated system never reaches 1300°C, there is no way to purposefully increase the oven temperature. The only option is to wait and hope the oven will eventually be able to accommodate higher temperatures.

9.5.4 Speed of temperature response

The under ventilated system has an advantage over the over ventilated system in that it reaches the desired temperature of 1300°C much faster. All under ventilated tests have reached this temperature within 5 minutes. The under ventilated tests quickly reach 1200°C and then gradually increase towards 1300°C, typically needing around ten minutes. However, implementing reference control in the over ventilated system will eliminate this advantage over time as the average heat flux imposed on the system reaches its goal value. If a short test duration is required though, the under ventilated system is favorable.

9.6 Automatic detection of ventilation state

The two options of oven builds results in two completely opposite system responses to input. A controller tuned to control the over ventilated system would therefore not be able to control an under ventilated system. With the system showing signs of being able to frequent both states in a single test, an algorithm that automatically detects the state of the system and changes between two controllers would be handy. A proposed approach would be to analyze the relationship between the fan input derivative and the temperature derivative throughout the test, or by analyzing the initial temperature transient.

As shown by the simulations of control on the mixed temperature model, running a PI controller tuned to control an over ventilated system on a system that is under ventilated at low fan inputs should be unproblematic. The controller can therefore be chosen prior to the test according to how the oven is built.

9.7 Noise filtering

The input sequence calculated by a PID control scheme when the maximum recorded temperature is used as the process variable fluctuates at a quite high frequency. This is caused by the noise in the process variable fed to the controller. Using this signal to control the fans would not be advantageous as it causes unnecessary stress on the fan motors. A smoother input signal works just as well, as can be seen by the test results from the PI controlled experiment, see chapter 6, where the controller used smooths the output generated. This is implemented in a PID scheme by lowpass filtering either the process variable fed to the controller, or the input sequence calculated by the PID algorithm. It is highly recommended that this should be done to avoid unnecessary strain on the fan motors.

Chapter 10

Conclusion

Through mathematical modeling, simulations and experimental testing, this thesis has worked towards determining a way to satisfyingly control both the temperature and heat flux in an oven used for testing equipments durability against jet fires. The two systems with different ventilation openings have been assessed and judged against each other to decide which is the most advantageous.

Simulation results suggests that a PI control scheme should be able to sufficiently control the ovens temperature in both systems, and this was confirmed by the experimental results for the over ventilated case. It is expected that PI control should work just as well in the under ventilated case. It is however important to note that the same controller would not work in both systems. Each system requires their own implementation of PI control.

Equal for both implementations of PI control is that either the process variable or the input calculated by the controller should be filtered to assure a smooth input signal controlling the fans. The controller for the over ventilated system also has to have an active integral anti-windup scheme to calculate input values within the allowed limits.

In addition to temperature control, control schemes for the temperature reference were proposed. Through simulations it was deduced that a simple P controller should be able to handle reference control successfully.

In the question of which of the two systems is more advantageous, the conclusion is not one sided. In many ways the two systems are both equal and opposite. They are expected to respond equally well to control, and their main problem is the exact opposite of each other. The under ventilated system has some advantages over the over ventilated system in that it utilizes the fuel more proficiently, and it does not produce black smoke. In addition, the temperature remains stable in a higher degree than the under ventilated system. The over ventilated system is thus the recommended setup, but should be reviewed continuously throughout challenging weather conditions. The advantage of the under ventilated

system is that it reaches the desired operating area quickly, and is less exposed to weather. Thus it could prove to be the better choice in certain weather conditions, or when a short test is required.

Bibliography

[1] Anti-Windup Control Using a PID Controller. https://se.mathworks.com/help/simulink/examples/anti-windup-control-using-a-pid-controller.html. Accessed: 2017-01-04.

[2] Google Earth. https://www.google.no/maps/@63.3577522,10.4251156,165m/data=!3m1!1e3?hl=en. Accessed: 2017-01-03.

[3] How Does the PID VI Handle Saturation Conditions? http://digital.ni.com/public.nsf/allkb/ACD4998DA4C74A3286257A760017E194. Accessed: 2017-01-04.

[4] Introduction to Thermocouples. http://www.capgo.com/Resources/Temperature/Thermocouple/Thermocouple.html. Accessed: 2016-12-06.

[5] ISO 22899-1:2007. http://www.iso.org/iso/catalogue_detail.htm?csnumber=39750. Accessed: 2017-01-12.

[6] Schneider Electric - Altivar 61. http://www.schneider-electric.com/en/product-range/1422-altivar-61/. Accessed: 2016-11-10.

[7] Thermocouples Operation & Maintenance Instructions. http://www.temperature.com.au/Support/Thermocouples/OperationMaintenanceInstructions.aspx. Accessed: 2016-12-06.

[8] What is Autoclaved Aerated Concrete (AAC)? http://www.aircrete-europe.com/en/aircrete-aac/what-is-autoclaved-aerated-concrete.html. Accessed: 2016-12-09.

[9] Ytong Porebetong. http://www.ytongsiporex.no/1763.php. Accessed: 2016-12-09.

[10] ABB. *1/4 DIN Process Controller - C351*, 2005.

[11] A. Ungut A.D. Johnson, L.C. Shirvill. CFD Calculation of Impinging Gas Jet Flames. Technical report, Health & Safety Executive.

[12] B.J. McCaffrey ans G. Heskestad. A robust bidirectional low-velocity probe for flame and fire application. *Combustion and Flame*, (26):125–127, 1976.

[13] P. Vandevelde B. Merci. Experimental study of a natural roof ventilation in full-scale enclosure fire tests in a small compartment. *Fire Safety Journal*, 42:523–535, 2007.

[14] C. Beyler. Analysis of Compartment Fires with Overhead Forced Ventilation. In B. Langford G. Cox, editor, *Fire Safety Science - Proceedings of the Third International Symposium*, pages 291–300, 1991.

[15] J.L. Bryan. *Fire suppression and detection systems*. Macmillan Publishing Co, 2 edition, 1982.

[16] Y.A. Cengel and J.M. Cimbala. *Fluid Mechanics - Fundamentals and Applications*. McGraw Hill, 2010.

[17] W.K. Chow. Modelling of Forced-Ventilation Fires. *Mathematical and Computer Modelling*, 18(5):63–66, 1993.

[18] L.W.D. Cullen. The public inquiry into the piper alpha disaster. *Drilling Contractor*, 49(4), 1993.

[19] C.V. Rao P.O.M. Scokaert D.Q. Mayne, J.B. Rawlings. Constrained model predictive control: Stability and optimality. *Automatica*, 36(6):789–814, 2000.

[20] D. Drysdale. *An indtroduction to fire dynamics*. John Wiley & Sons. Inc, 1998.

[21] R.D. Braatz E.L. Russel, L.H. Chiang. Fault detection in industrial processes using canonical variate analysis and dynamic principal component analysis. *Chemometrics and Intelligent Laboratory Systems*, 51(1):81–93, 2000.

[22] F. Incropera et al. *Fundamentals of Heat and Mass transfer*. John Wiley & Sons, 2011.

[23] M. Gómes-Mares et al. Jet fires and the domino effect. *Fire safety journal*, 43(8):583–588, 2008.

[24] K. Matsuyama et.al. A Simple Predictive Method for Room Fire Behaviour. *Fire Science & Technology*, 18(1):23–32, 1998.

[25] C. Hugget. Estimation of heat release by means of oxygen consumption method. *Fire and Materials*, 4(2):61–65, 1980.

[26] N.J. Alvares J. Backovsky, K.L. Foote. Temperature profiles in Forced-Ventilation Enclosure Fires. In Y. Hasemi, editor, *Fire Safety Science - Proceedings of the Fifth International Symposium*, pages 403–414, 1997.

[27] I.B. Lee J.M. Lee, S.J. Qin. Fault detection and diagnosis based on modified independent component analysis. *AIChE Journal*, 52(10):3501–3514, 2006.

[28] L.A. Kent and M.E. Schneider. The design and application of bi-directional velocity probes for measurements in large pool fires. *ISA Transactions*, 26(4):25–32, 1987.

[29] G. Liebe. *Brannfysikk*. Norsk Brannvernforening, 1995.

[30] C.L. Beyler M.J. Peatross. Ventilation Effects on Compartment Fire Characterization. In Y. Hasemi, editor, *Fire Safety Science - Proceedings of the Fifth International Symposium*, pages 403–414, 1997.

[31] National Instruments. *Temperature Measurements with Thermocouples: How-To Guide*, December 2011.

[32] J.G. Quintiere P. Sharma. Compartment Fire Temperatures. *Journal of Fire Protection Engineering*, 20:253–271, 2010.

[33] D.M. Himmelblau R. Luo, M. Misra. Sensor Fault Detection via Multiscale Analysis and Dynamic PCA. *Industrial & Engineering Chemisty Research*, 38(4):1489–1495, 1999.

[34] J. A. Rockett. Fire Induced Gas Flow in an Enclosure. *Combustion Science and Technology*, 12:165–175, 1976.

[35] H.M. Sandvik. Modeling and control of temperature in a jet fire test rig. Project thesis, Norwegian University of Science and Technology.

[36] J.M. Lee J.Y. Park I.B. Lee S.W. Choi, C. Lee. Fault detection and identification of nonlinear processes based on kernel PCA. *Chemometrics and Intelligent Laboratory Systems*, 75(1):55–67, 2005.

[37] M. Sato T. Tanaka and T. Wakamatsu. Simple formula for ventilation controlled fire temperatures. In K.A. Beall, editor, *Thirteenth meeting of the UJNR panel on fire research and safety*, volume 1, June 1997.

[38] T. Tanaka and K. Nakamura. A model for predicting smoke transport in buildings - based on two layer zone concept. *Report of The Building Research Institute Occasional Report*, (123), 1989.

[39] P.H. Thomas W.D. Walton and Y. Ohmiya. *SFPE Handbook of Fire Protection Engineering*, chapter 30, pages 996–1023. Springer, 5 edition, 2016.

Appendix

A Model parameter values

Global parameters

Table A1: Global parameters used in all models and approximations.

Parameter	Value	Unit	Description
c_p	1.005	kJ/kgK	Specific heat of air
ρ_∞	1.225	kg/m^3	Density of ambient air
σ	5.67·10^{-11}	kW/m^{2}K^4	Stefan-Boltzmann constant
ΔH_p	27100	kJ/kg	Heat released per unit mass of propane
ΔH_a	3000	kJ/kg	Heat released per unit mass of air
ε_W	1		Wall emissivity constant
c_r	0.5	kg/sm$^{5/2}$	Natural ventilation constant
V	21.84	m^3	Inner oven volume
A_{tot}	46.96	m^2	Total inner area of oven (including openings)
r_{fan}	0.2	m	Radius of fan shafts

Ventilation opening areas in tests

Table A2: Ventilation opening areas in all tests.

Date	A_{op_v} [m^2]	A_{op_h} [m^2]	A_W [m^2]
13.10.15	3.75	0	43.21
22.10.15	3.75	0	43.21
28.10.15	3.75	0	43.21
30.10.15	3.75	0	43.21
14.04.16	3.75	0	43.21
12.05.16	5.68	3.12	38.16
28.06.16	9.36	3.12	34.48
29.06.16	9.36	3.12	34.48
30.06.16	9.36	3.12	34.48
01.07.16	6.24	3.12	37.60
26.10.16	5.68	3.12	38.16

B Measurement data from under ventilated tests

13.10.2015

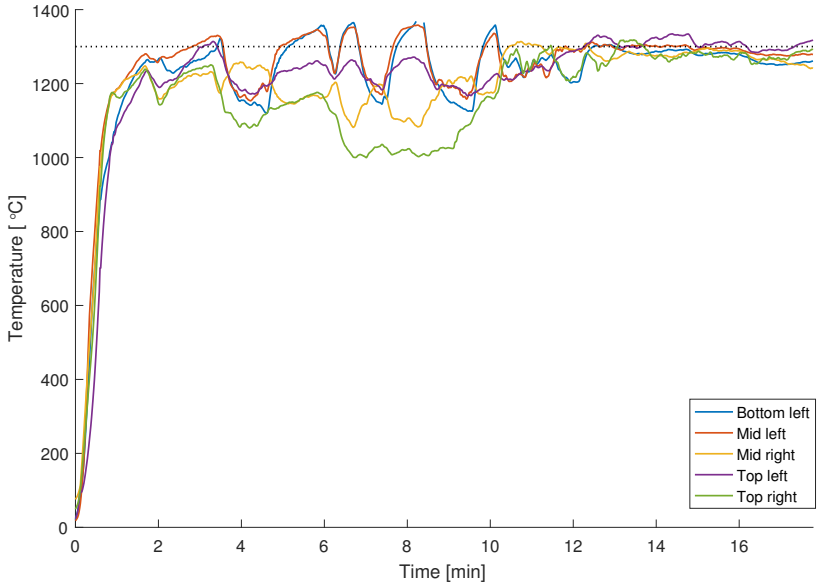

(a) Temperature measurements 13.10.2015.

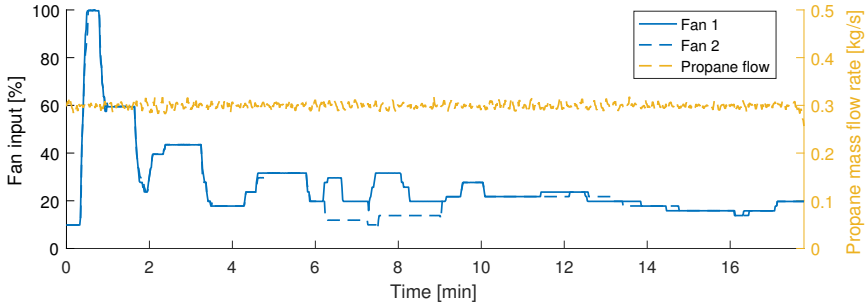

(b) Fan and propane inputs 13.10.2015.

Figure B1: Measurement data from 13.10.2015.

22.10.2015

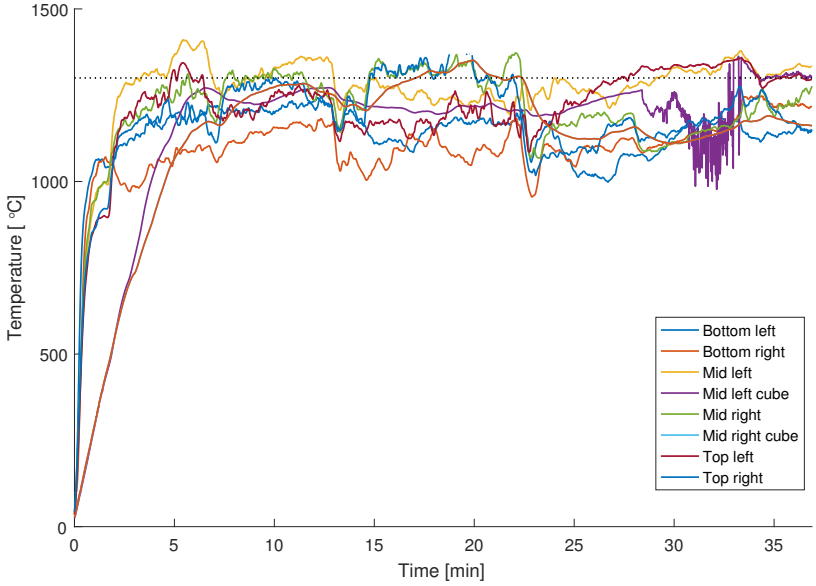

(a) Temperature measurements 22.10.2015.

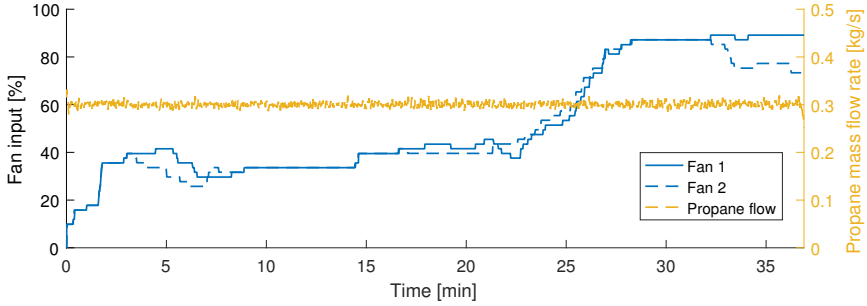

(b) Fan and propane inputs 22.10.2015.

Figure B2: Measurement data from 22.10.2015.

28.10.2015

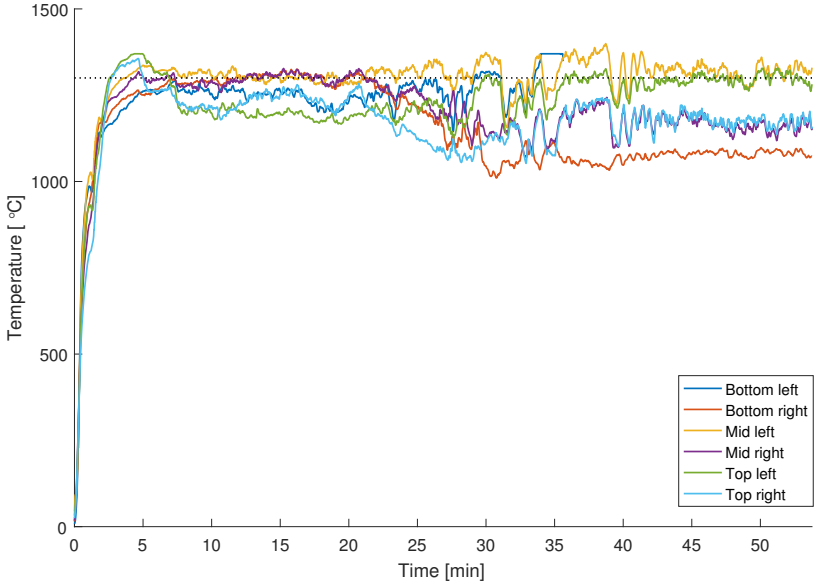

(a) Temperature measurements 28.10.2015.

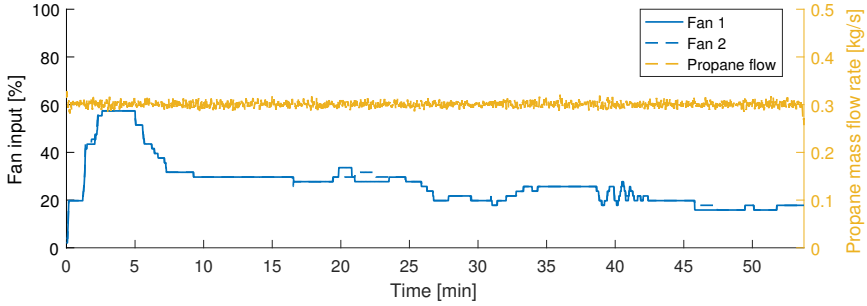

(b) Fan and propane inputs 28.10.2015.

Figure B3: Measurement data from 28.10.2015.

30.10.2015

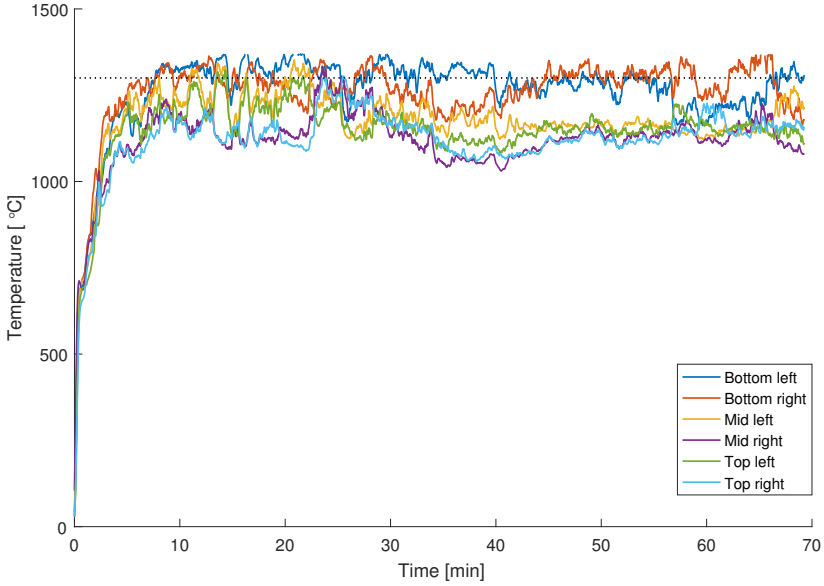

(a) Temperature measurements 30.10.2015.

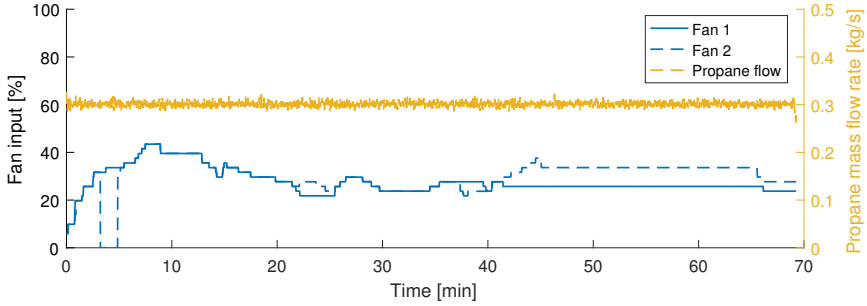

(b) Fan and propane inputs 30.10.2015.

Figure B4: Measurement data from 30.10.2015.

14.04.2016

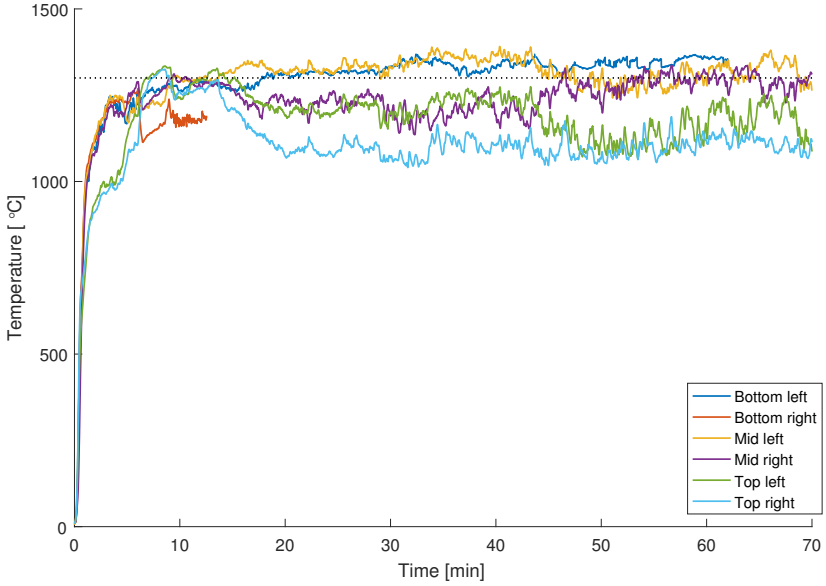

(a) Temperature measurements 14.04.2016.

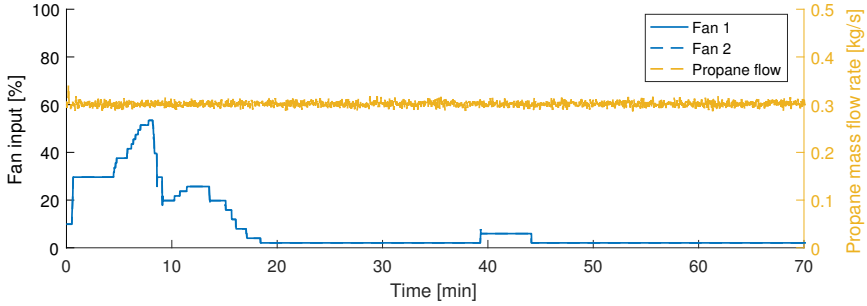

(b) Fan and propane inputs 14.04.2016.

Figure B5: Measurement data from 14.04.2016.

C Measurement data from over ventilated tests

12.05.2016

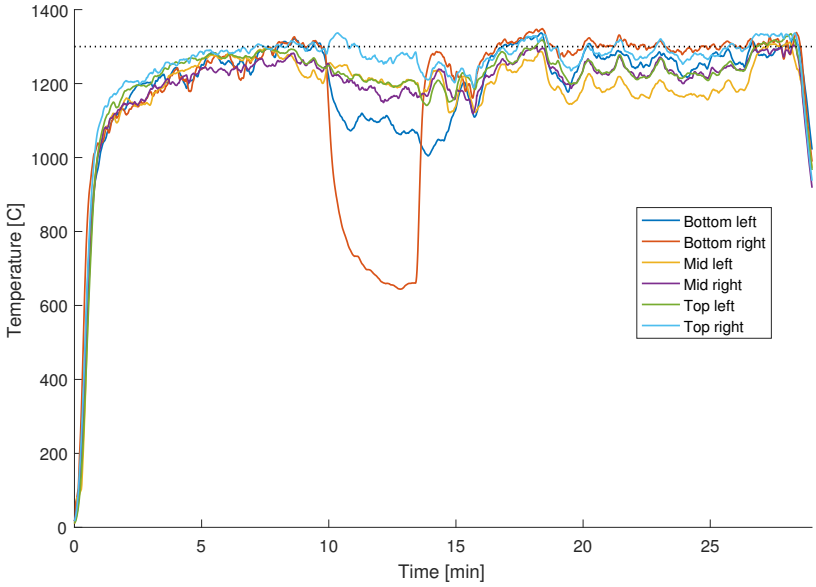

(a) Temperature measurements 12.05.2016.

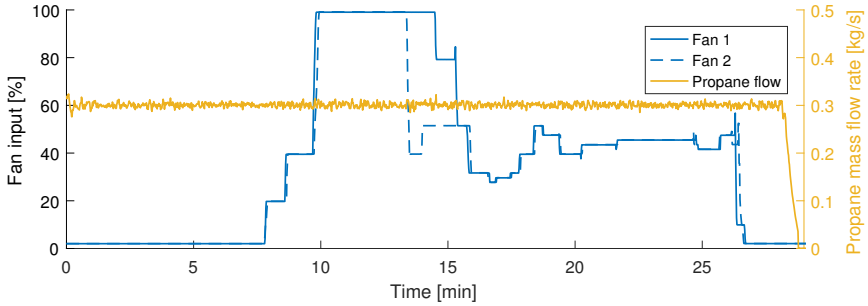

(b) Fan and propane inputs 12.05.2016.

Figure C1: Measurement data from 12.05.2016.

28.06.2016

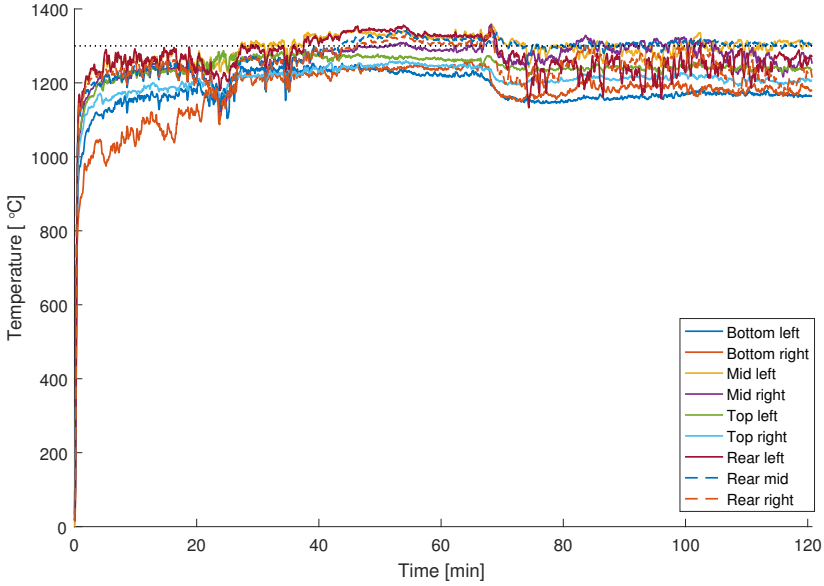

(a) Temperature measurements.

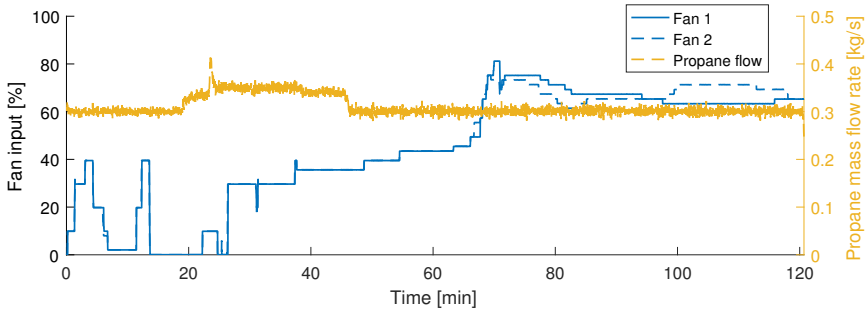

(b) Fan and propane inputs.

Figure C2: Measurement data from 28.06.2016.

29.06.2016

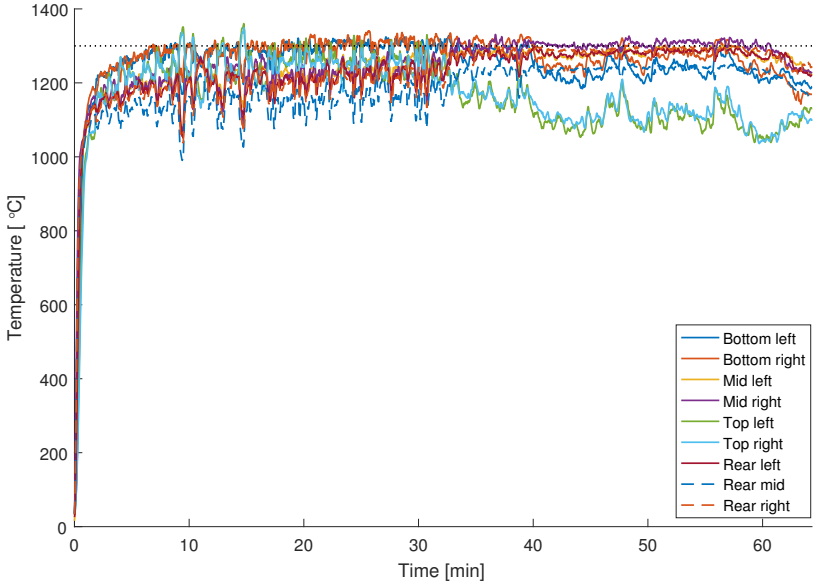

(a) Temperature measurements.

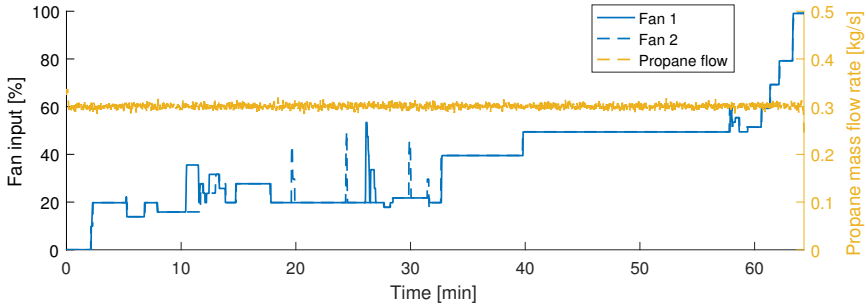

(b) Fan and propane inputs.

Figure C3: Measurement data from 29.06.2016.

30.06.2016

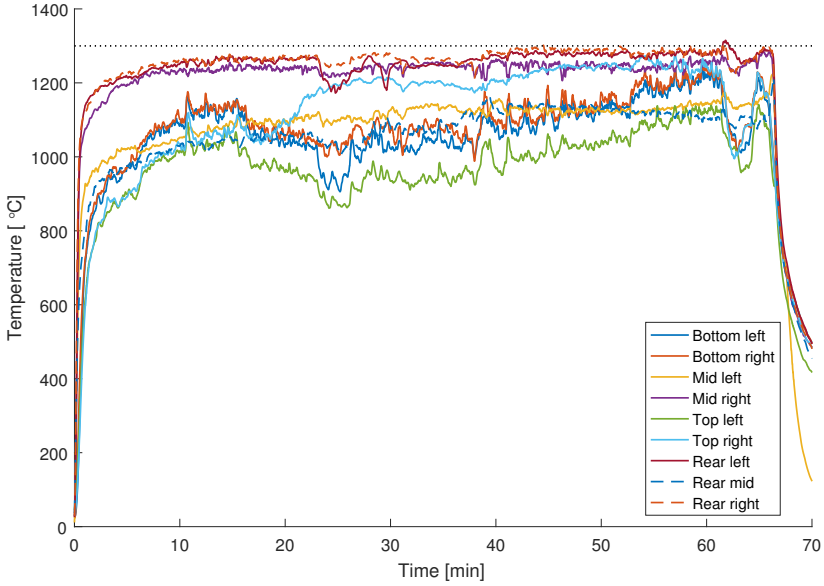

(a) Temperature measurements.

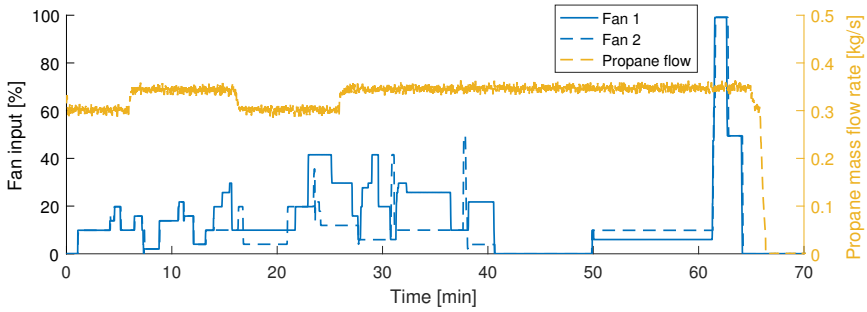

(b) Fan and propane inputs.

Figure C4: Measurement data from 30.06.2016.

01.07.2016

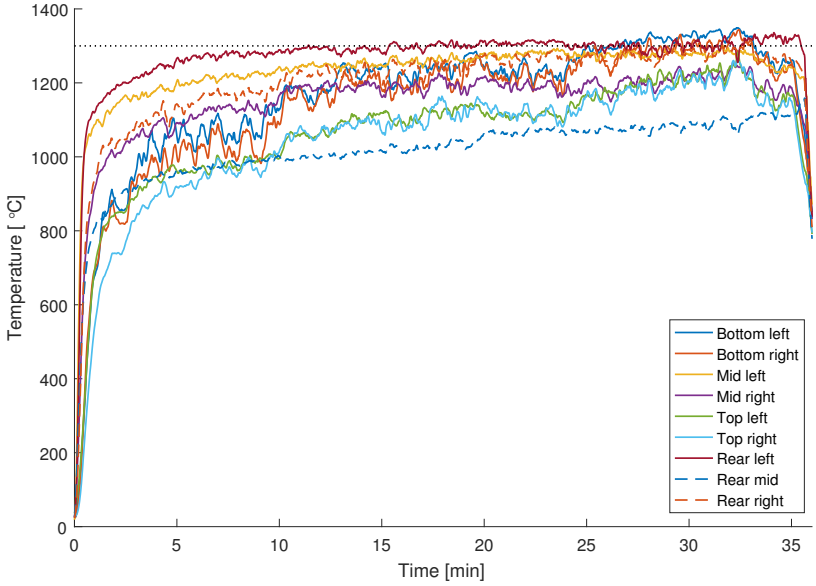

(a) Temperature measurements.

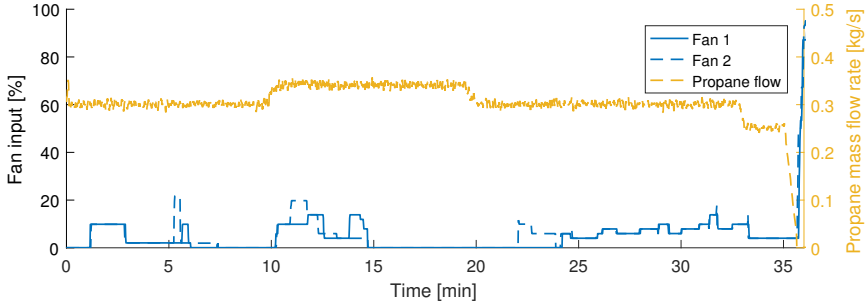

(b) Fan and propane inputs.

Figure C5: Measurement data from 01.07.2016.

D Weather data all tests

Wind 13.10.2015

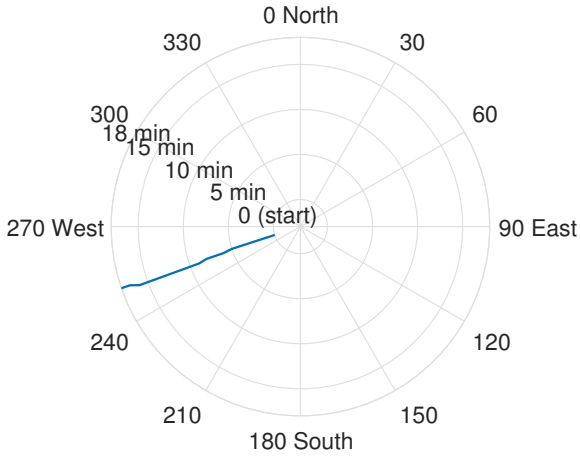

(a) Wind bearing.

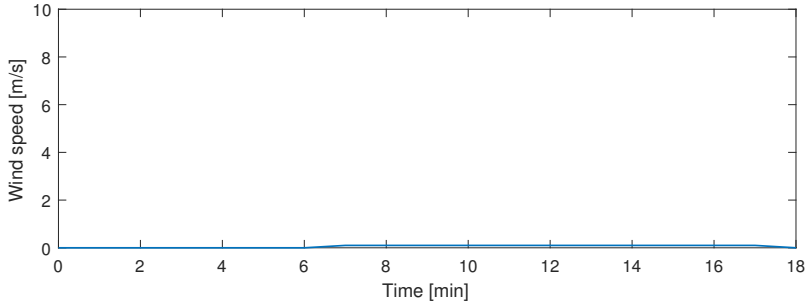

(b) Wind speed.

Figure D1: Measured wind speed and bearing 13.10.2015.

Wind 22.10.2015

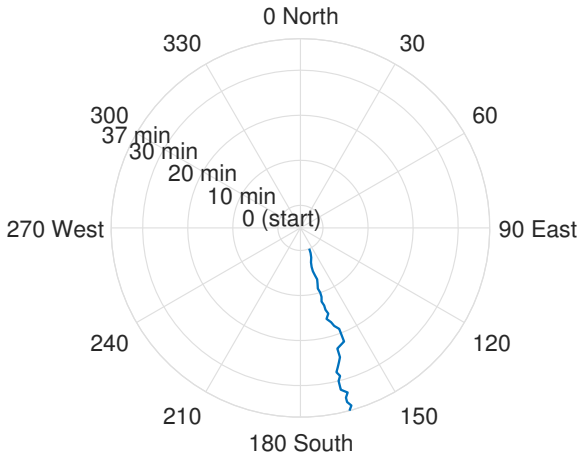

(a) Wind bearing.

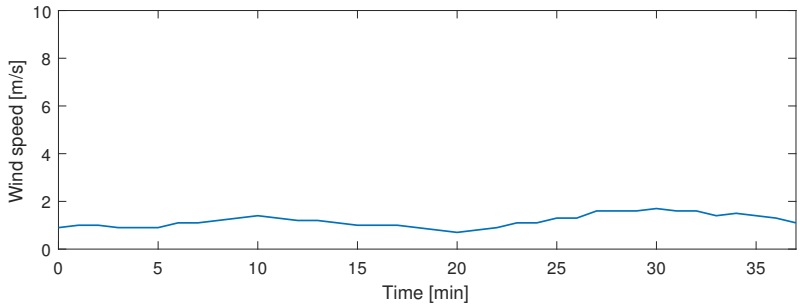

(b) Wind speed.

Figure D2: Measured wind speed and bearing 22.10.2015.

Wind 28.10.2015

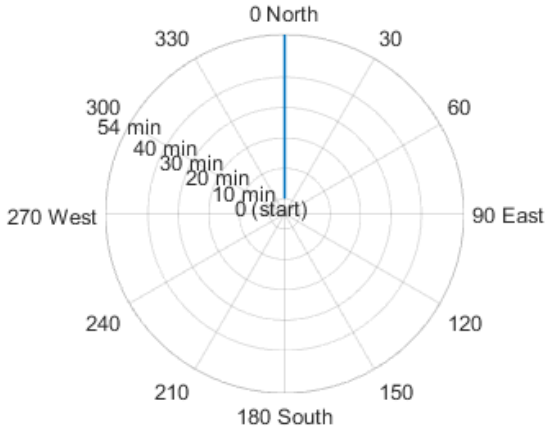

(a) Wind bearing.

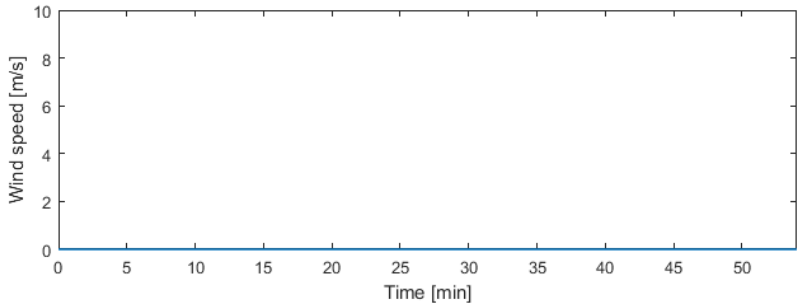

(b) Wind speed.

Figure D3: Measured wind speed and bearing 28.10.2015.

Wind 30.10.2015

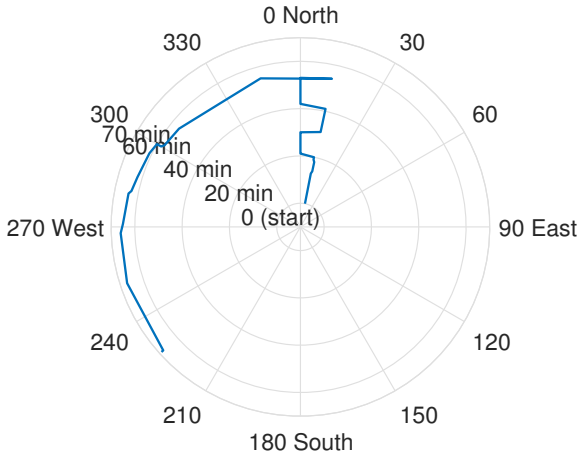

(a) Wind bearing.

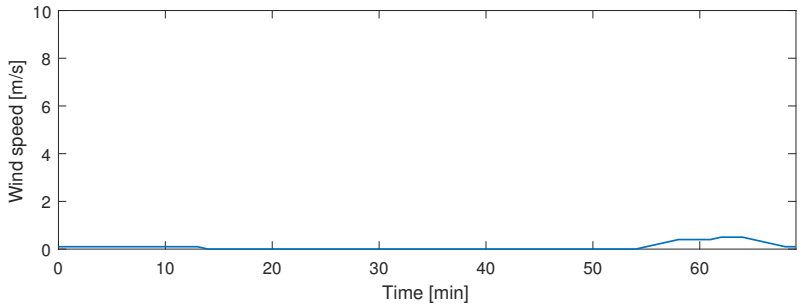

(b) Wind speed.

Figure D4: Measured wind speed and bearing 30.10.2015.

Wind 28.06.2016

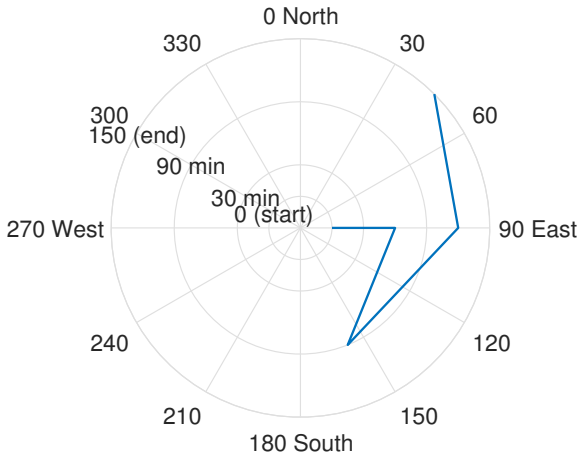

(a) Wind bearing.

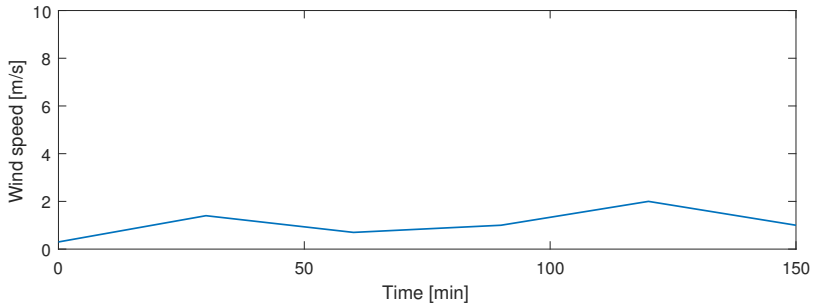

(b) Wind speed.

Figure D5: Measured wind speed and bearing 28.06.2016.

Wind 29.06.2016

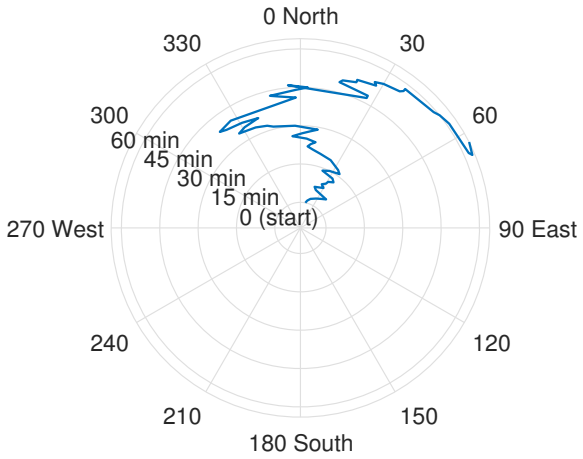

(a) Wind bearing.

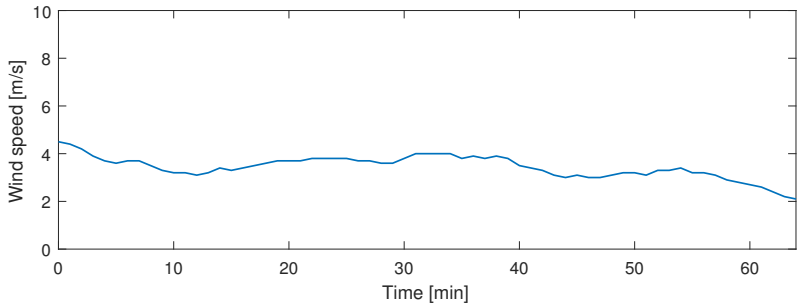

(b) Wind speed.

Figure D6: Measured wind speed and bearing 29.06.2016.

Wind 30.06.2016

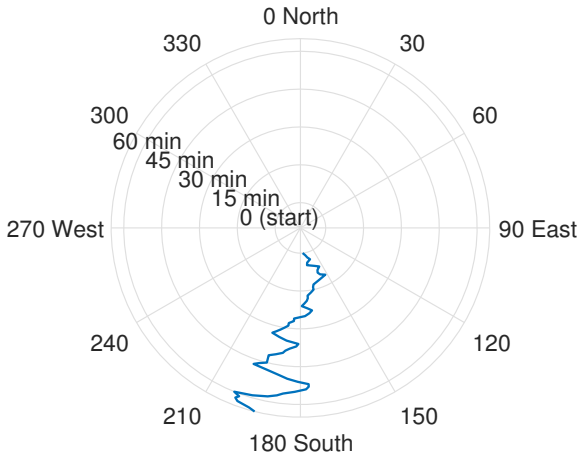

(a) Wind bearing.

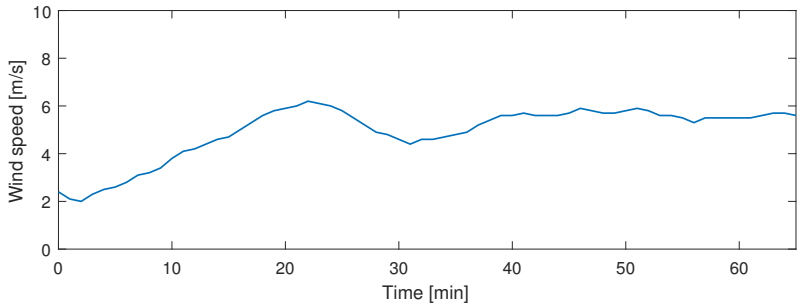

(b) Wind speed.

Figure D7: Measured wind speed and bearing 30.06.2016.

Wind 01.07.2016

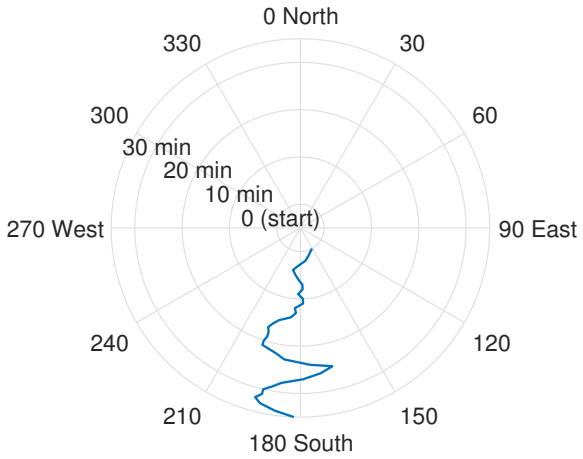

(a) Wind bearing.

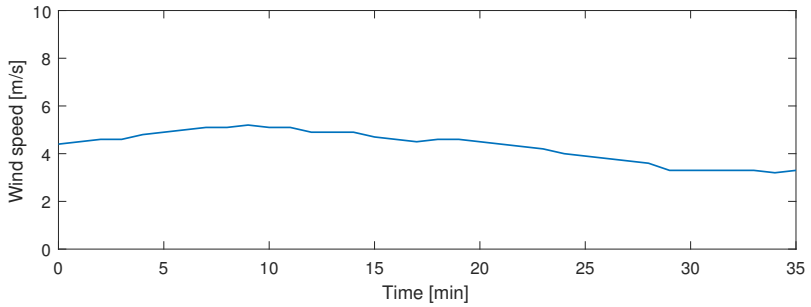

(b) Wind speed.

Figure D8: Measured wind speed and bearing 01.07.2016.

Other weather data

Table A3: Various weather data from all tests

Date	Temperature	Humidity	Rainfall today
13.10.15	7.6	88.4	0.0
22.10.15	12.4	69.8	2.8
28.10.15	3.0	96.0	0.2
30.10.15	3.9	89.2	0.2
28.06.16	18.2	51.2	3.9
29.06.16	20.5	42.3	0.0
30.06.16	21.1	38.8	0.0
01.07.16	22.9	29.4	0.0

E MATLAB files

A .zip file is available online containing MATLAB and Simulink files created in this thesis. Table E1 gives an overview of the files contained in this .zip file. MATLAB R2016a or a newer version is required to run some of the files.

Table E1: Overview of files in .zip file.

File name	Extension	Description
Measurement data		Folder containing Excell sheets with all available measurement data
fan_calibration	.m	Script for plotting results of fan calibration
fan_data	.m	Values used in fan_calibration
mixed_vent_MPC	.m.	Script for simulating and plotting MPC control
mixed_vent_MPC_sim	.slx	Simulink diagram MPC control
mixed_vent_PID_reg	.m	Script for simulating and plotting PID control
mixed_vent_PID_reg_sim	.slx	Simulink diagram PID control
mixed_vent_ramp	.m	Plots the mixed ventilated systems response to ramped input
mixed_vent_sim	.slx	Simulink diagram for the mixed ventilation model
mpc_controllers	.mat	Contains the MPC controller used in mixed_vent_MPC
over_vent_sim	.slx	Simulink diagram for the over ventilated model
over_vent_step	.m	Plots the over ventilated models step response
txxxxxx_parameters	.mat	Parameter values used to recreate temperature on date xxxxxx
temperature_noise	.mat	Contains noise sequence used in control simulations
under_vent_sim	.slx	Simulink diagram for the under ventilated model
under_vent_step	.m	Plots the under ventilated models step response